ELSEVIER

Sensors and Actuators B 73 (2001) 1–26

SENSORS AND ACTUATORS B CHEMICAL

www.elsevier.nl/locate/sensorb

Micromachined metal oxide gas sensors: opportunities to improve sensor performance

Isolde Simon[a], Nicolae Bârsan[b,*], Michael Bauer[a], Udo Weimar[b]

[a]Robert Bosch GmbH, Automotive Equipment Division K8, Tübinger Street 123, 72703 Reutlingen, Germany
[b]Institute of Physical and Theoretical Chemistry, Morgenstelle 8, D-72076 Tübingen, Germany

Received 4 July 2000; received in revised form 20 August 2000; accepted 23 August 2000

Abstract

This review deals with gas sensors combining a metal oxide based sensing layer and a substrate realized by using micromachining. It starts by giving an overview of the design principles and technology involved in the fabrication of micromachined substrates examining thermal and mechanical aspects. Both kinds of micromachined substrates, closed-membrane-type and the suspended-membrane-type, are discussed. The deposition of the sensing layer is complicated by the mechanical fragility of the micromachined substrates. Different approaches used for the formation of the sensing layer such as thin film and thick film deposition techniques are reviewed. Finally, the gas sensing function of the sensitive layer is analyzed and various ways for extracting the information are presented with respect to the improvement of sensor performance brought by this new approach.

Keywords: Micro gas sensors; Micromachining; Metal oxide

1. Introduction

Gases are linked to life and their odors tremendously influence the `image' of our environment. The human nose serves as a highly advanced sensing instrument which is able to differentiate between hundreds of smells but fails if absolute gas concentrations or odorless gases need to be detected. The demand for gas sensing devices which support the human nose is accordingly large. Support is desired in safety applications where combustible or toxic gases are present and in comfort applications, such as climate controls of buildings and vehicles where good air quality is required. Additionally, gas monitoring is needed in process control and laboratory analytics.

Only for process control and laboratory analytics one can afford high performance, large and expensive gas analyzers. For all other purposes one misses either the money or the place for gas analyzers. Therefore one needs cheap, small and user-friendly gas sensing devices. Accordingly, a lot of research and development is done to design small and cheap gas sensors which possess high sensitivity, selectivity and stability with respect to a given application. This search comes along with a large variety of sensors based on different sensing principles, e.g. semiconductor gas sensors, optical sensors, thermal conductivity sensors, mass sensitive devices like quartz microbalance sensors, catalytic sensors, dielectric sensors, electrochemical sensors and electrolyte sensors.

The focus of this paper is on semiconductor gas sensors based on metal oxides. Their advantages are good sensitivity to some relevant gases like CO, H_2, NO_x and hydrocarbons, simple signal processing, low production cost and small size. Metal oxide gas sensors are frequently used in gas leakage detection (propane, butane) and ambient air quality monitoring in traffic (CO, NO_x). The latter application utilizes a metal oxide sensor to close the air intake in the presence of high concentrations of noxious gases. New application fields are toxic gas detection, like CO, and smoke gas monitoring in houses and buildings.

Well known materials used in metal oxide gas sensors are SnO_2, ZnO, TiO_2 and WO_3, but SnO_2 is by far the most popular. All those materials are n-type semiconductors which have, under normal atmospheric conditions and typical working temperatures in 200–400°C range, an electron depleted surface. Electron depletion at the surface is due to adsorption of atmospheric oxygen as O_2^- or O^- species which tie up electronic carriers. The electron depleted

* Corresponding author. Tel.: +49-7071-29-78765; fax: +49-7071-29-5960.
E-mail addresses: isolde.simon@de.bosch.com (I. Simon), nb@ipc.uni-tuebingen.de (N. Bârsan).

0925-4005/01/$ – see front matter
PII: S0925-4005(00)00639-0

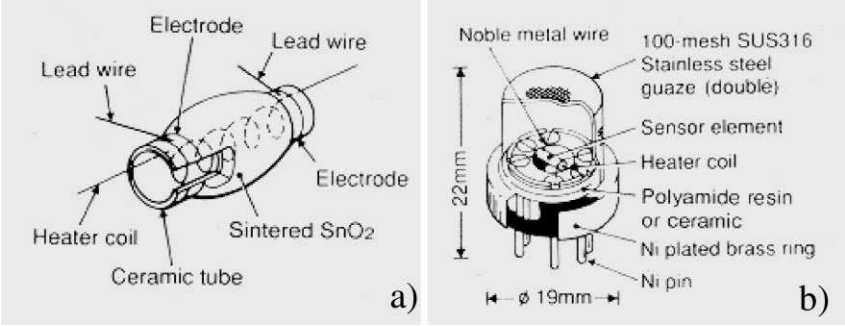

Fig. 1. Taguchi-type sensor [95]. (a) Sensor Element: the heater is embedded in an alumina ceramic tube and the semiconductor material is mounted on the tube with two printed gold electrodes. The heater is needed to achieve the typical sensor working temperatures in 200–400°C range and the two electrodes allow the measurement of gas sensitive changes in electrical conductivity. (b) Packaged Sensor: the heated sensor element is mounted such that thermal contact between substrate and element is only given via the connecting wires.

surface is highly gas sensitive: reducing gases like CO or H_2 react with the surface removing the chemisorbed oxygen such that the depletion region decreases, oxidizing gases like NO_2 cause an increase of the depletion region. The microscopic changes in the depletion region strongly influence the electrical properties. Measurements of changes in the electric conductivity therefore often serve as sensor signal.

The idea of using semiconductors as gas sensitive devices leads back to 1952 when Brattain and Bardeen first reported gas sensitive effects on Germanium [1]. Later, Seiyama found gas sensing effect on metal oxides [2]. Taguchi finally brought semiconductor sensors based on metal oxides to an industrial product [3–5]. Taguchi-type sensors are still on the market, a typical example is given in Fig. 1, but most of the commercially available sensors are nowadays manufactured in screen printing technique on small and thin ceramic substrates [6–8], an example is given in Fig. 2. Screen-printing technique has the advantage that thick-films of metal oxide semiconductor sensors are deposited in batch processing thus leading to a small sensor to sensor distribution within production lots. This technology is nowadays well-established and high performance of screen-printed ceramic sensors is achieved in various field applications.

However, screen-printed ceramic gas sensors are, with respect to power consumption, mounting technology and selectivity still in need of improvement. The power consumption of screen-printed devices is typically in the range of 200 mW to about 1 W [6]. That is too much for applications which allow just the use of battery-driven elements. The mounting of the overall hot ceramic element is difficult. One has to find such designs like the one shown in Fig. 2 which ensure good thermal isolation between sensor element and housing as well as high mechanical stability. Good thermal isolation is thereby not only needed to minimize the overall power consumption but also to enable the integration of signal processing electronics in the same housing. Sufficient selectivity of metal oxide sensors can up to now only be achieved if the sensor is used in an application where the number of gases is limited such that cross-sensitivities can be neglected or if several sensors are put together to an array. In the latter case a lack of selectivity and therefore overlapping sensitivities of different sensors can be turned into an advantage [9]. Even though the use of arrays is very promising with respect to sensor selectivity one has to have in mind that the use of sensor arrays leads at the same time either to an increased size of the sensor element or to the use of several separate sensor elements and thus to an increased power consumption.

In the last years the above-mentioned difficulties lead to new developments in substrate technology and strong research in preparation of sensing materials and signal evaluation. The integration of gas sensitive metal oxide layers in standard microelectronic processing was achieved

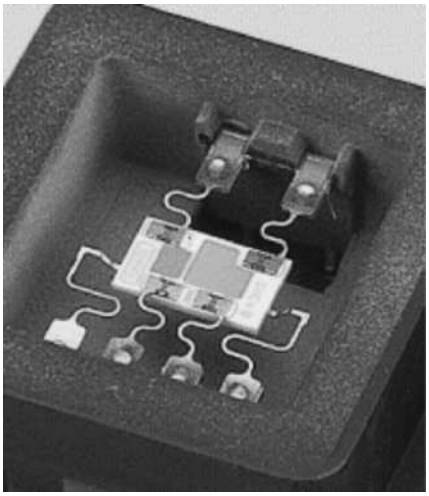

Fig. 2. Gas sensor prepared by screen-printing on a ceramic substrate of size 6 mm × 3 mm [89]. The sensor element consists of a CO- and a NO_x-sensitive layer. The platinum structures (heater, electrodes and contact pads) and the two sensitive layers are manufactured in screen-printing technology. The sensitive layers consist of specifically doped and coated tin dioxide. Their electrical resistance is measured by interdigitated platinum electrodes located below the sensitive layers and the necessary sensor working temperature of about 300°C is achieved by a heater located on the backside of the ceramic. With help of the platinum contact pads the sensor is fixed to a steel leadframe by parallel gap welding and mounted in the housing.

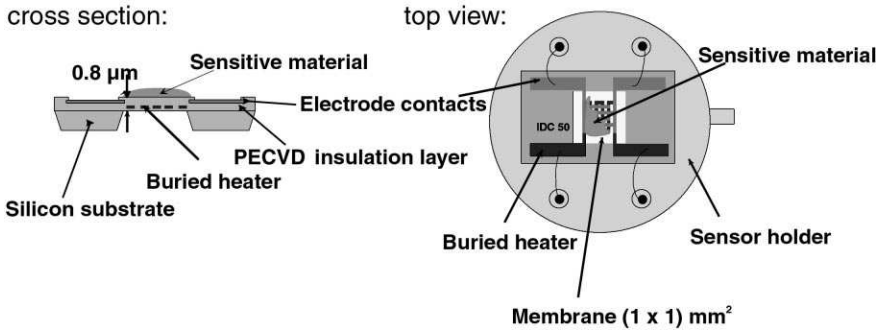

Fig. 3. Schematic of IPC microsensor. The sensitive film was deposited by drop deposition onto the micromachined substrate. The membrane consists of stress-free LPCVD silicon nitride and platinum as heater and electrode material.

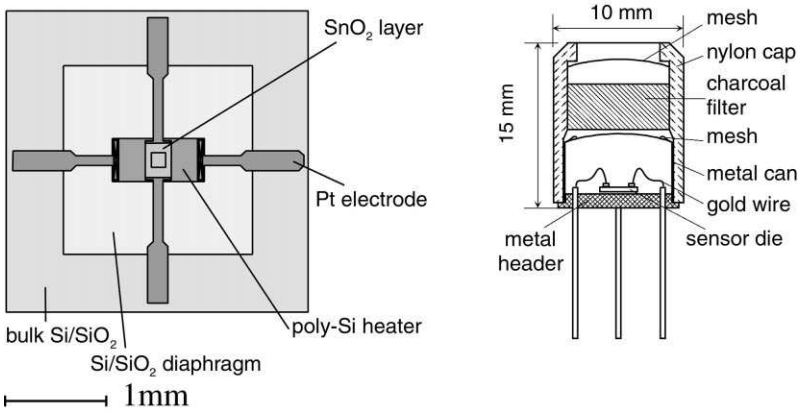

Fig. 4. Schematic of the MGS 1100 sensor from Motorola. Micromachined sensor element on the left and sensor housing on the right. The sensitive film were obtained by rheotaxial growth and thermal oxidation of tin layers (RGTO) deposited on the silicon oxide–nitride membrane.

and lead together with the use of micromachining steps to micromachined metal oxide gas sensors like the ones shown in Figs. 3 and 4.[1] This technology is very promising to overcome the difficulties of screen-printed ceramic sensors due to the following facts. The sensitive layer of micromachined metal oxide gas sensors is deposited onto a thin dielectric membrane of low thermal conductivity which provides good thermal isolation between substrate and the gas-sensitive heated area on the membrane. In this way the power consumption can be kept very low (typical values obtained lie in the range between 30 and 150 mW [10–12]) and the substrate itself stays nearly at ambient temperature. The mounting of the sensor element becomes therefore much easier than for an overall hot ceramic sensor element, and control and signal-processing electronics can be integrated on the same substrate if desired. Using standard microelectronic steps to pattern electrode structures results in a further advantage. The minimal structure sizes get much smaller, a minimal width between electrodes lying in the mm range can be achieved [13]. The gas sensitive area can in this way be tremendously reduced and the use of interdigitated electrodes with a high length-to-width ration allows even the evaluation of sensing films with very high sheet resistivity. Sensor arrays which are often needed to overcome the bad selectivity of single sensor elements can be easily implemented in this technology. Beyond that, the small thermal mass of each micromachined element allows rapid thermal programming which can be used to study the kinetics of surface processes and to achieve kinetically controlled selectivity [14].

This paper reviews the research and developments established so far in the field of micromachined metal oxide gas sensors. This includes a description of frequently used technologies, a discussion of design parameters which influence the thermal and mechanical properties of such devices and finally a description of the actual gas sensing principles. All these aspects are interconnected. Fig. 5 visualizes the various interactions. The properties of the sensor element such as mechanical stability, power consumption and thermal response are mainly determined by the different parts of the sensor element. Details of these interactions are given in Sections 2 and 3. Additionally the sensor parts have a strong influence on the actual gas

[1] IPC: Institute of Physical and Theoretical Chemistry, Morgenstelle 8, D-72076 Tübingen; Motorola gave the chemical sensor business up in 1998, but the technology is now used by the company Micro Chemical Systems SA (MICS).

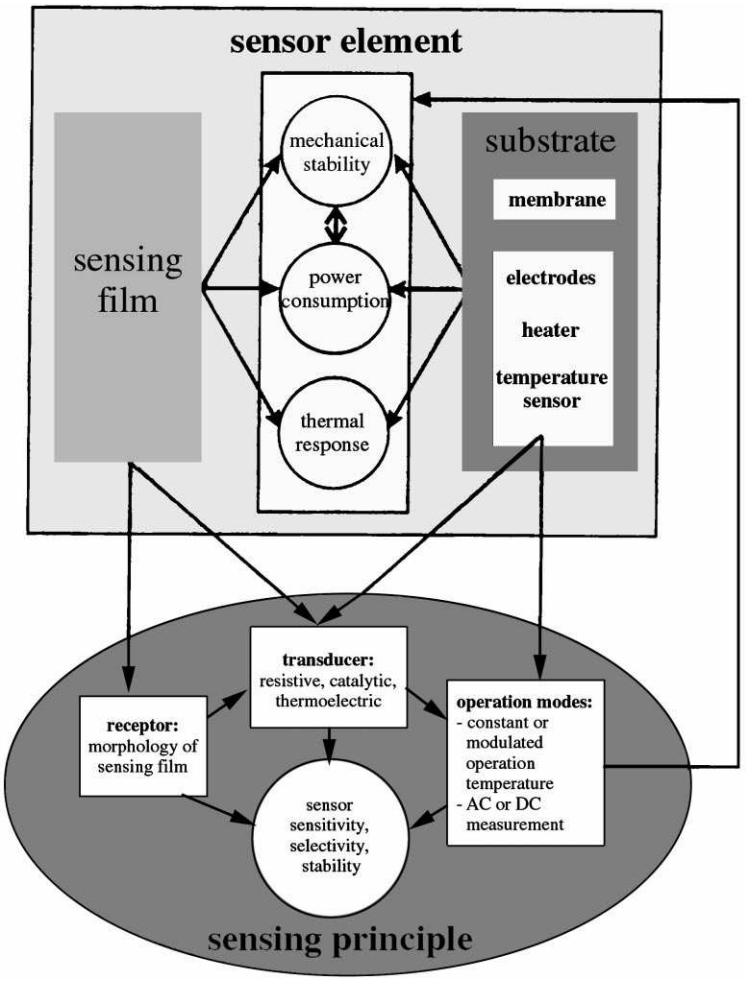

Fig. 5. Schematic of the various interactions between different sensor parts, thermal and mechanical properties, and the actual gas sensing of a micromachined gas sensor. Interactions with sensor housing and mounting technology are not shown in this context.

sensing. The choice of sensing ®lm is responsible for the receptor function of the sensor, i.e. the speci®c reaction between gas species and the ®lm, and determines together with other sensor parts how such gas reactions are transduced into a measurable sensor signal. The gas sensing by itself is very complex. By combination of various transducer and operation modes one can create a large variety of sensor signals. Some possibilities and their effect on the properties of the sensor element are described in Section 4.

Before going into details it should be emphasized that not only the proper design of the micromachined gas sensor element but also the proper choice of packaging solutions and mounting technologies is absolutely necessary to obtain ®nally a gas sensor systems which can withstand the harsh environment of practical applications, e.g. shock, vibration, ambient temperature changes and so on. Even though this paper deals only with the micromachined gas sensor chip one should have in mind that this chip has to be designed such that it can be mounted on a substrate, electrically connected and packaged.

2. Micromachining substrates for gas sensors

To fabricate micromachined gas sensors, sensor substrate materials have to be chosen and functional elements have to be designed. This is complicated by the lack of reliable material constants for thin ®lms. This section presents typical designs found in literature and describes some criteria for the design of substrates with low power consumption, well-controlled temperature distribution across the sensing layer, and high mechanical strength. Well-controlled temperature distributions over the sensing layer are desired as the sensing properties of metal oxides are strongly temperature dependent. Generally the goal is a uniform temperature distribution but sometimes thermovoltages are used as sensor signal requiring well-controlled temperature gradients. High mechanical strength is needed for all processing steps used to form the micromachined substrate. Beyond that, the micromachined substrate should be stable during the deposition of the sensing ®lm and subsequent processing.

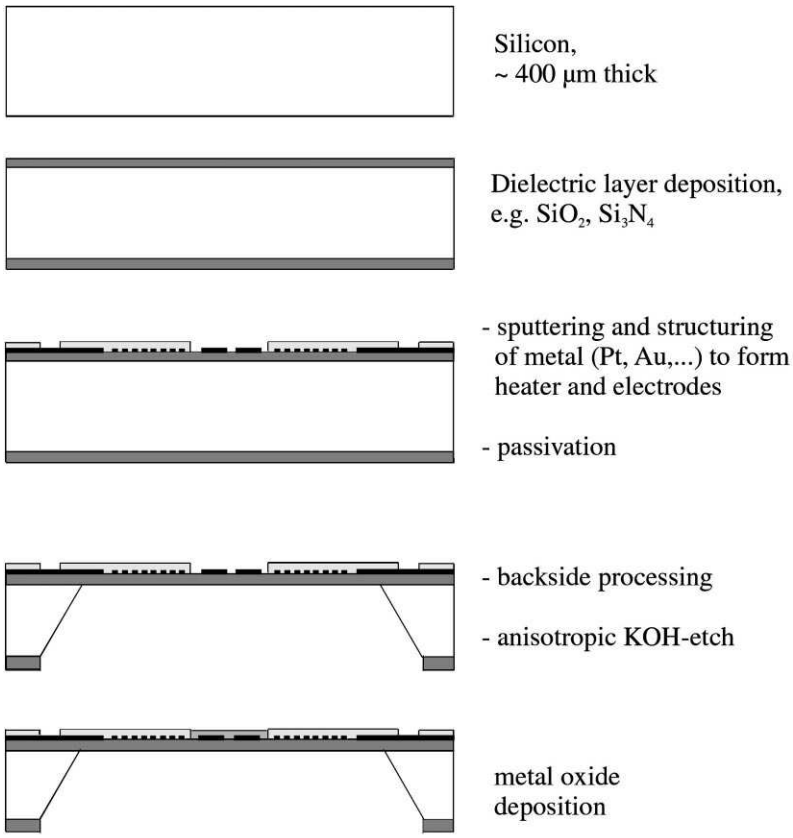

Fig. 6. Schematic process flow for the formation of a closed-membrane type gas sensor.

2.1. Technology

2.1.1. Formation of closed and suspended membranes

The starting point for the production of micromachined gas sensors is silicon in all cases. A typical process flow is sketched in Fig. 6. Basically there are two different structures for micromachined gas sensors using metal oxide as the sensing material. One is the closed-membrane-type gas sensor and the other the suspended-membrane-type gas sensor, which is also called spider-type gas sensor. Schematic views of those structures are presented in Figs. 7 and 8.

The closed-membrane-type sensor is formed by anisotropic etching of silicon from the backside. Wet etchants like KOH or EDP[2] are generally used. Appropriate etch stops for those etchants are silicon nitride, silicon oxide or Boron-doped silicon. For the formation of the membrane two different strategies are known. The first, the more popular one, uses silicon oxide and/or silicon nitride as membrane and insulation materials to obtain membranes of typical thickness between 1 and 2 mm [12,15,16]. The second, lately demonstrated, uses nitrided porous silicon of thickness between 25 and 30 mm [17] which can be obtained by silicon anodization and following nitridation. Silicon oxide, silicon nitride and nitrided porous silicon posses all low thermal conductivities (Table 1) and can thus provide good thermal isolation between the heated active area and the membrane rim. Silicon nitride layers generally have large tensile stress and silicon oxide layers are compressive. Nevertheless, by appropriate choice of deposition and annealing steps multilayer systems of silicon oxide and/or silicon nitride have been proven mechanically stable. In the case of nitrided porous silicon Maccagnani et al. [17] could use screen-printing technique to print SnO_2-paste on the formed membranes thus demonstrating high mechanical strength. The process flow for formation of the membrane is in either case fully IC-compatible. A disadvantage lies in the need of double-side alignment for the bulk silicon etch from the backside, and the sloped side-walls obtained by anisotropic etching. The sloped side-walls make the lateral dimensions needed to form a membrane a factor $\sqrt{2}$ larger. Plasma etching techniques like high rate silicon etching which can form vertical walls might therefore be an alternative to wet etching making a higher number of sensors on a wafer possible.

The suspended-membrane-type is completely processed from the front-side. Therefore, the suspended membrane is often claimed to be more compatible with CMOS process [18]. The suspended membrane is either formed by anisotropic etch with KOH or EDP from the front [18,19] or by sacrificial etching. In case of anisotropic etching, the mem-

[2] Ethylenediamine-pyrocatechol-pyrazine in water solution.

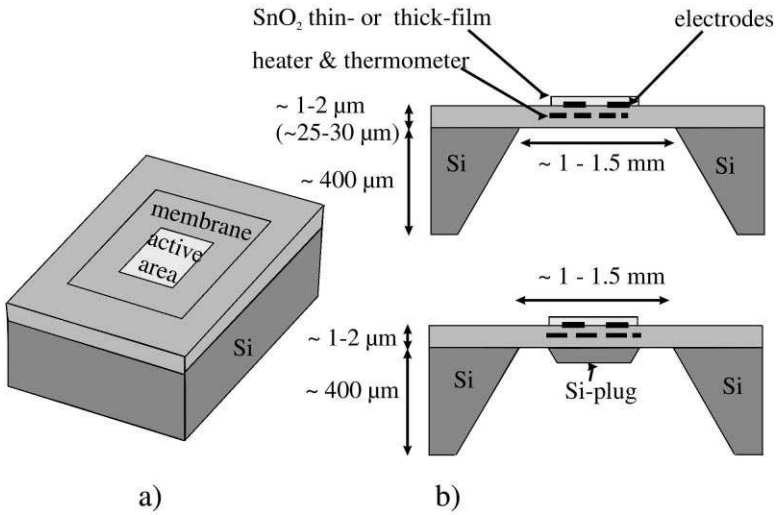

Fig. 7. Schematic of closed-membrane-type gas sensor: (a) top view; (b) side view.

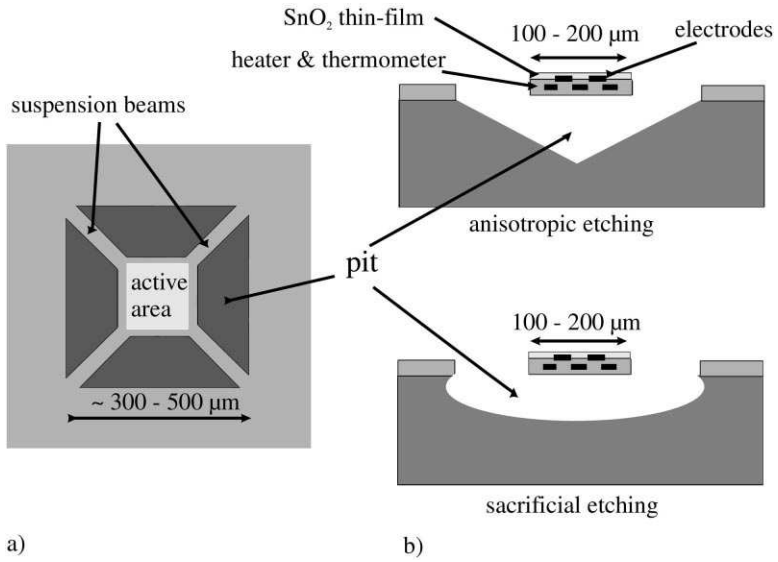

Fig. 8. Schematic of suspended-membrane-type gas sensor: (a) top view; (b) side view.

Table 1
Thermal conductivity and capacity of substrate materials and air[a]

Material	Modification	T (K)	Thermal conductivity ($W\,m^{-1}\,K^{-1}$)	Thermal capacity ($10^6\ J\,m^{-3}\,K^{-1}$)	References
Silicon	Undoping	300	150	1.63	[87]
	Doping (10^{19} atoms per cm^3)	n.s.	50, 70	±	[32]
Nitrided porous silicon	55% Porosity	n.s.	0.74±4.09	±	[17]
Silicon oxide	n.s.	300	1.4	1.61	[40]
Silicon nitride	n.s.	300	9±30	1.86±2.48	[40]
Polysilicon	(10^{20} atoms per cm^3)	n.s.	29±34	±	[32]
	n-Doping (10^{20} atoms per cm^3)	n.s.	16±24	±	[32]
	p-Doping (10^{20} atoms per cm^3)	n.s.	17±20	±	[32]
Platinum		293	70	2.85	[88]
Diamond	n.s.	300	1000, 2000	±	[29,40]
Silicon carbide	n.s.	300	121±500	±	[40]
Air		293	0.026	±	[35]
		593	0.044	±	[35]

[a]Thermal conductivity and capacity of substrate materials and air. Modifications and temperatures are listed as specified in the cited references; n.s. stands for not specified.

brane is first formed by dielectric layers like silicon oxide and/or nitride and patterned to form etch windows. The etching is performed afterwards, or after dicing and packaging [18] to avoid the harsh environment during the dicing process. Sacrificial etching of porous silicon is another possibility to obtain suspended membranes [20,21]. Dücsö et al. [20] use selective formation of porous silicon in a p-type silicon wafer to obtain an undercut profile below implanted n-type silicon regions. The formed membrane consists of of a 5 mm thick n-type silicon plate hanging on suspension beams formed by 1.6 mm thick silicon nitride. Due to the high thermal conductivity of silicon (Table 1) the silicon membrane provides good temperature uniformity of the active area and shows excellent mechanical stability. The typical lateral dimensions of suspended membranes lie between 100 and 200 mm.

2.1.2. Integration of electrodes, heater and thermometer

Metal electrodes, deposited on top of the formed membranes in the so-called active area, make the measurement of the gas sensitive layer resistance possible. Generally, the electrodes are thereby located underneath the sensing film, but the deposition of so-called top electrodes on thin gas-sensitive tin oxide layers has also been realized [13]. Usually, the electrode materials are gold [15] and platinum [16,22], in some cases also aluminum or wolfram [19,23] have been used. Aluminum is advantageous as it is the standard metallization in IC-processes, but its contact properties to the sensing film are rather bad and maximum operation temperature is limited to about 500°C due to thermal migration and oxidation. To achieve good adhesion of the electrodes adhesion layers are often necessary. Chung et al. [22] use, for example, 20 nm Ti as adhesion layer for deposition of platinum.

Heater and thermometer structures which are needed to control the sensor operation temperature can be integrated in two different ways. In case that platinum or gold are used as electrode materials, heater and thermometer structures can be integrated in the same layer as the electrodes. This approach is known as horizontal approach and sketched in Fig. 9b. An advantage of the horizontal approach is that no additional process steps are needed to form heater and thermometer structures. On the other hand, the design of structures which guarantee as well appropriate resistance measurements as well-defined temperature distributions over the active area might be quite a challenge. The design in a vertical approach, where heater and thermometer are formed in different layers as depicted in Fig. 9a, allows much more freedom. Heater and thermometer are frequently formed by polysilicon, platinum or p^{++}-doped structures, sometimes the heater and thermometer are one and the same. Polysilicon can be introduced by standard CVD process and photolithographic patterned. The same holds for platinum which is easily sputtered and patterned by lift-off process or ion beam etching. Whereas polysilicon structures can be easily integrated in an IC-process, platinum structures are generally not [16]. Polysilicon, as well as platinum, are embedded in silicon oxide or nitride for electrical isolation. Appropriate thickness for polysilicon are about 0.5 mm [24,25]. Sheet resistance of the polysilicon can be adjusted by n-type doping with $POCl_3$ [25] and it is possible to fabricate polysilicon with negative temperature coefficient resistance (TCR). This is a large advantage compared with platinum heaters as negative TCR materials counteract to hot spots whereas heater materials with a positive TCR like platinum have an amplifying effect on hot spots [11]. Hot spots are critically with respect to heater degradation and sensing properties of metal oxide.

Boron-doped (p^{++}) silicon might be an alternative to platinum and polysilicon. The structures are formed below the membrane and serve during the etching process as p^{++} etch stop. A disadvantage of p^{++} structures are the high doping rates necessary for the formation of an p^{++} etch stop. Due to incorporation of the smaller radius Boron atoms in the silicon crystal structure, high mechanical stresses are induced causing distortions (bending, buckling) in the etched structures [26].

Thermometers have been also realized by aluminum plates with electrical connections for four-point temperature measurement [19] or by forward biased p–n-junctions as the voltage of such constant current diodes is directly proportional to the absolute temperature [27,28]. The use of aluminum plates improves additionally the temperature uniformity over the active area, but limits on the other side the sensor operation and annealing temperatures to values below 500°C.

In addition to the active layers, silicon plugs beneath the membrane as depicted in Fig. 7 or high thermal conducting

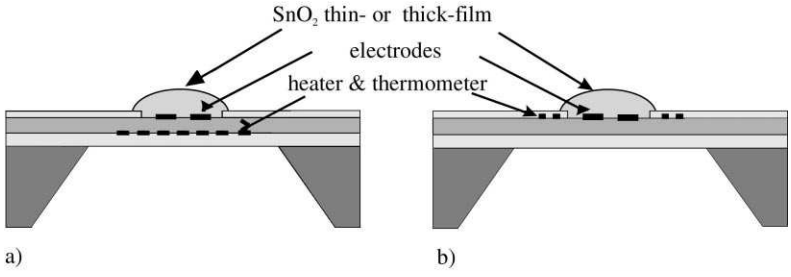

Fig. 9. (a) Vertical and (b) horizontal approach.

thin films like weakly doped diamond or silicon carbide [29] are sometimes introduced to improve temperature uniformity. Silicon plugs of about 10 mm thickness can be formed either by heavily Boron-doping for plug definition [11] or by use of two KOH etching steps [30]. Diamond or silicon carbide layers are more difficult to obtain due to their exceptional growth behavior. They can be generated by a modified SIMOX (separation by ion implantation of oxygen) process [29].

2.2. Thermal design

The thermal characteristics of micromachined gas sensors have to be optimized with respect to low power consumption, well-controlled temperature distribution over the sensing layer and fast transient response, if the sensor is intended to be temperature modulated.

2.2.1. Pathways of heat transfer: total power consumption

Heat transfer occurs due to heat conduction, heat convection and radiation. In Fig. 10 the different heat flow components are marked. Along the membrane one has to deal with heat conduction. Above and below the membrane heat transfer occurs due to heat conduction and heat convection through the surrounding atmosphere. Additionally, radiation has to be taken into account.

According to the different pathways of heat transfer the determination of the total heat loss and temperature distribution is not an easy task. An experimental approach which allows to get a feeling for the different pathways of heat transfer is the measurement of total heat loss in vacuum. In vacuum one has only to deal with heat losses due to conduction along the membrane and radiation. By taking advantage of the different temperature dependencies of conduction (T-linear in temperature) and radiation (T^4-dependency) one can easily separate between those two components [25]. One can thus determine both the heat loss due to conduction along the membrane and the heat loss due to radiation. This method works pretty well for devices already available but can hardly be used to design new devices. In this case, simple models for basic understanding are necessary and, to minimize the costs of development, extensive simulation studies like FEM-simulations are required.

Assuming that the different components of heat flow are additive, the total heat flow can be expressed as

$$Q_{tot} = G_m \lambda_m (T_{hot} - T_{amb}) + G_{air} \lambda_{air} (T_{hot} - T_{amb}) + G_{rad} \varepsilon \sigma (T_{hot}^4 - T_{amb}^4) + x \quad (1)$$

The first term describes the heat conduction through the closed membrane, the second the heat conduction through the ambient air, the third heat losses due to radiation and the last term accounts for unknown heat losses including free convection. G_m, G_{air} and G_{rad} are geometry factors and are empirical values which contain information about the geometry of the closed or suspended membrane and its effect on heat losses. T_{hot} and T_{amb} denote the temperature of the hot active area, respectively, the ambient; λ_m, λ_{air} are the thermal conductivity of the membrane and the surrounding atmosphere, ε the emissitivity and σ the Stefan–Boltzmann constant. In the next sections the different terms are discussed and expressions for the geometry factors are obtained.

2.2.1.1. Heat conduction through the membrane.

For the calculation of the heat conduction one has to deal with a three-dimensional problem. For simplification, the heat conduction perpendicular to the membrane is generally neglected, which seems reasonable due to the dimensions of the membrane: thickness several mm, edge length about 1 mm. In case of a suspended membrane, a further reduction to a one-dimensional problem is straightforward as heat conduction occurs basically only along the suspension beams with length l and sectional area of A_{beam}. Conduction within the membrane plate is negligible in comparison [10]. For the suspended membrane, one obtains in the case of four suspension beams

$$Q_{membrane} = \frac{4 \lambda_m A_{beam} (T_{hot} - T_{amb})}{l} \quad (2)$$

$$G_m = \frac{4 A_{beam}}{l} \quad (3)$$

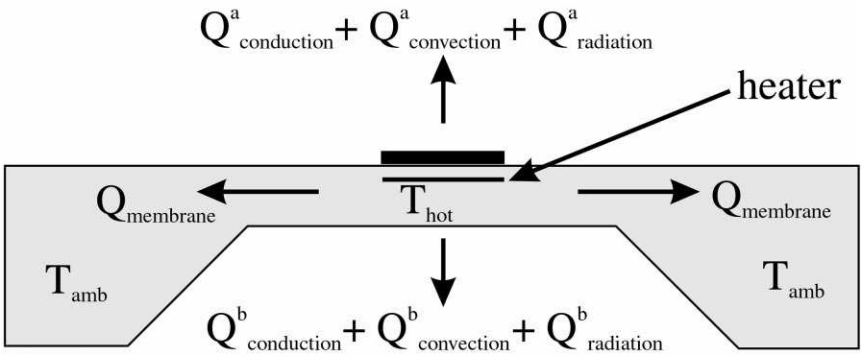

Fig. 10. Heat fluxes of a micromachined gas sensor.

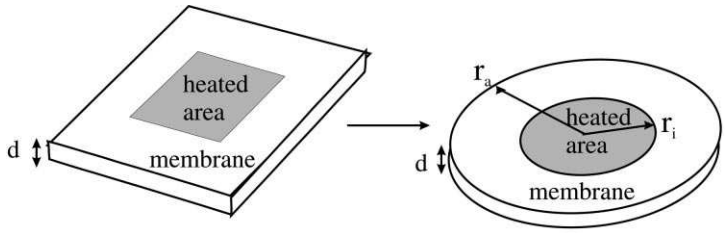

Fig. 11. Reduction to one-dimensional heat conduction.

For closed membranes, a simple model is obtained by replacement of the square membrane by a round one [12] as depicted in Fig. 11. This leads to a one-dimensional heat conduction problem in cylindrical coordinates which can be easily solved [31],

$$Q_{membrane} = \frac{2\pi\lambda_m d (T_{hot} - T_{amb})}{\ln(r_a/r_i)} \quad (4)$$

$$G_m = \frac{2\pi d}{\ln(r_a/r_i)} \quad (5)$$

where d denotes the thickness of the membrane, r_i and r_a the radii of the heated and the membrane area.

One can clearly see from Eqs. (2) and (4) that the choice of membrane/suspension beam materials of low thermal conductivity and small thickness is desirable to achieve low thermal losses. In Table 1 some thermal conductivities are listed illustrating, for example, why silicon despite of its mechanical strength should be avoided as membrane/suspension beam material. The actual total thermal conductivity of a n-multilayer system is thereby given by $\lambda_m \sum_{i=1}^{n} \lambda_i d_i / \sum_{i=1}^{n} d_i$.

Length to width ratio of the suspension beams, respectively, the relation r_a/r_i should additionally be chosen as large as possible to minimize heat losses. But whereas the suspension beams show a linear dependency on length to width ratio the relation r_a/r_i influences the heat losses of a closed membrane in a logarithmic scale as presented in Fig. 12.

This result is in line with FEM-simulations and experimental data. Simulations from Götz et al. [11] show that the power consumption as a function of distance between heated area and silicon rim for a heater size of about 500 μm × 500 μm decreases with increasing distance but, and that is important, for a distance exceeding 400 μm (corresponding to $r_a/r_i > 2{:}6$) the thermal isolation is practically not improved further, i.e. there exists a lower limit of power consumption for a given heater size. Similar experimental and simulated results are presented by Astie et al. [32] using also a heater of 500 μm × 500 μm. They could reduce the heat losses due to conduction along the membrane from 67 to 31% of the total dissipated energy by replacing a 0:8 mm × 0:8 mm membrane by a 1:8 mm × 1:8 mm membrane. The importance of adequate scaling of the square heating resistor (edge length a) compared with the square membrane (edge length b) is also mentioned by Lee et al. [16], they selected a ratio of $b{:}a = 3{:}1$ to keep heat losses low.

Putting some reasonable numbers in Eqs. (2) and (4), e.g. choosing $\lambda_m = 10\ W\ m^{-1}\ K^{-1}$, $d = 2\ \mu m$, $T_{hot} - T_{amb} = 300\ K$ one obtains in case of suspension beams with typical length 100 μm and width 20 μm a heat loss of 4.8 mW, for a closed membrane with ratios $r_a/r_i = 2$, 5 and 8 heat losses of 54, 23 and 18 mW, respectively. The suspended membrane type is thus with respect to heat losses through the membrane, respectively, the suspension beams clearly the favorite.

2.2.1.2. Heat losses to the air. Heat losses to the surrounding air can occur due to two different mechanisms, i.e. fluid motion and conduction. Fluid motion can either be caused by external forces or it can be the result of temperature differences which lead to density variations in the gravitational field and thus to buoyancy forces. The former case leads to heat transfer called forced convection, the latter is called free or natural convection. When there is no fluid motion, heat is transferred only by conduction.

In the following it is assumed that no external forces are applied, i.e. forced convection is excluded. Nevertheless, due to the coupling of the temperature field with the density field and thus the fluid field, the calculation of heat losses to the air remains difficult. Therefore, calculations are often

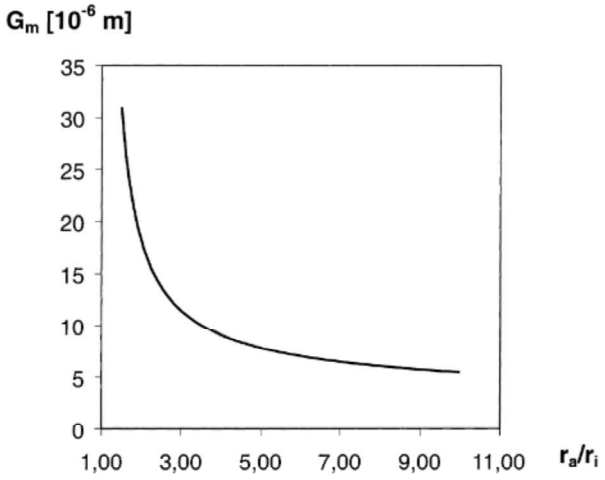

Fig. 12. Geometry factor for closed membrane of thickness 2 μm determined for cylindrical symmetry.

simplified. In literature one can find two different approaches for simplification. In the first approach, fluid motion is neglected. In the second approach heat transfer is described with help of empirical heat transfer coefficients.

The first approach is used by many authors [10,11,25,33]. They assume that there is no significant contribution of convectional fluid motion because of the small size of the heated structures and take into account for heat transfer to the air only the heat conduction. The validity of this assumption is supported by FEM-simulations from Sberveglieri et al. [12] and Götz et al. [34] which show that the differences in simulated heat loss considering fluid motion and disregarding it are only about 5%. Due to this result it seems reasonable to solve only the heat conduction problem neglecting any fluid motion.

Under this assumption one can use the following simple model as an estimate for heat losses to the air. This model [12] approximates the hot gas sensor and the cold ambient by concentric spheres with radii r_i and r_a yielding

$$Q_{conduction} = \frac{4\pi\lambda_{air}(T_{hot} - T_{amb})}{1/r_i - 1/r_a} = 4\pi r_i \lambda_{air}(T_{hot} - T_{amb}) \quad (6)$$

$$G_{air} = 4\pi r_i \quad (7)$$

Such a spherical geometry can be used as the equi-temperature surfaces in the far field of any body in three-dimensional space are `normally' spheres. The difference between r_a and r_i should be chosen comparable with the smallest distance between hot gas sensitive layer and cold surrounding elements. In the common case that the outer radius r_a is large compared with the inner r_i the second line of Eq. (6) gets valid. Thus, to optimize the power consumption the heated area represented by the inner radius r_i should be minimized as much as possible.

This model is a rather rough estimate as the actual cold surrounding elements do not lie on an outer sphere at all and the distances, heated area, membrane rim as well as heated area, die, respectively, pit depth (in case of suspended membrane), lie in the same range or are even smaller than the inner radius of the heated area. For example, for the backside of the membrane it might be more appropriate to describe the hot membrane area A and the cold die, respectively, cold bulk silicon with planar geometry

$$Q^b_{conduction} = \frac{\lambda_{air} A (T_{hot} - T_{amb})}{h} \quad (8)$$

where h denotes the distance between die and membrane, respectively, the pit depth.

Therefore, to solve the heat conduction problem more correctly, numerical solutions, as discussed in Section 2.2.4, are necessary. They take the different positions of the cold surrounding elements into account and solve the three-dimensional problem with these boundary conditions. An additional fact dealing with conduction in air which needs to be considered is the temperature dependence of the thermal conductivity of air, e.g. $\lambda(20\,^\circ C) = 0.026\,W\,K^{-1}\,m^{-1}$, $\lambda(320\,^\circ C) = 0.044\,W\,K^{-1}\,m^{-1}$ [35]. This temperature dependence cannot be neglected and illustrates that heat losses to the air are not only a function of the temperature difference between cold ambient and hot active area but depend on absolute temperature.

From the above discussion one can conclude that heat losses to the air can be best minimized by minimization of the heated area, maximization of the distance between cold die and hot membrane and choice of low operation temperature.

Qualitatively the same results are obtained with the second approach which takes fluid motion into account. In this case empirical heat transfer coefficients are used to describe the heat losses to the air. Heat transfer coefficients are, in general, empirical values and account for heat transfer due to conduction as well as fluid motion. They are defined as proportional constants between the heat flow density j_q and the temperature difference between a solid body and a fluid. The total heat flow Q_{air} from a heated membrane area to the surrounding air can thus described as

$$Q_{air} = \alpha_m A (T_{hot} - T_{amb}) \quad (9)$$

with α_m being the mean heat transfer coefficient. Theoretical determination of heat transfer coefficients requires knowledge of the temperature field and the velocity field and is rather difficult. However, for certain problems one can find empirical equations describing heat transfer. Such an equation for the heated membrane can be found by modeling the heated membrane area as a horizontal plate of characteristic size l. In this case the mean heat transfer coefficient above the hotplate is given by

$$\alpha_m = \frac{Nu\,\lambda(T_m)}{l} \quad (10)$$

with $\lambda(T_m)$ denoting the thermal conductivity at $T_m = (T_{hot} + T_{ambient})/2$ and Nu the Nusselt number. The Nusselt number is, with the assumption of laminar flow, i.e. for Rayleigh and Prandtl numbers

$$Ra\,f_2(Pr) < 7 \cdot 10^4 \quad \text{and} \quad 0 < Pr < 1 \quad (11)$$

given by

$$Nu_m = 0.766\,(Ra\,f_2(Pr))^{1/5} \quad (12)$$

with

$$f_2(Pr) = \left(1 + \left(\frac{0.322}{Pr}\right)^{11/20}\right)^{20/11} \quad (13)$$

Details for calculation can be found in [31,36,37].

Characteristic results for heat transfer above various hotplates are shown in Fig. 13. Similar results can be obtained for heat transfer below hotplates. But due to the boundary conditions at the back of the heated membrane, i.e. cavern and die, the modeling of the heated membrane with a horizontal plate which posses no boundary conditions seems

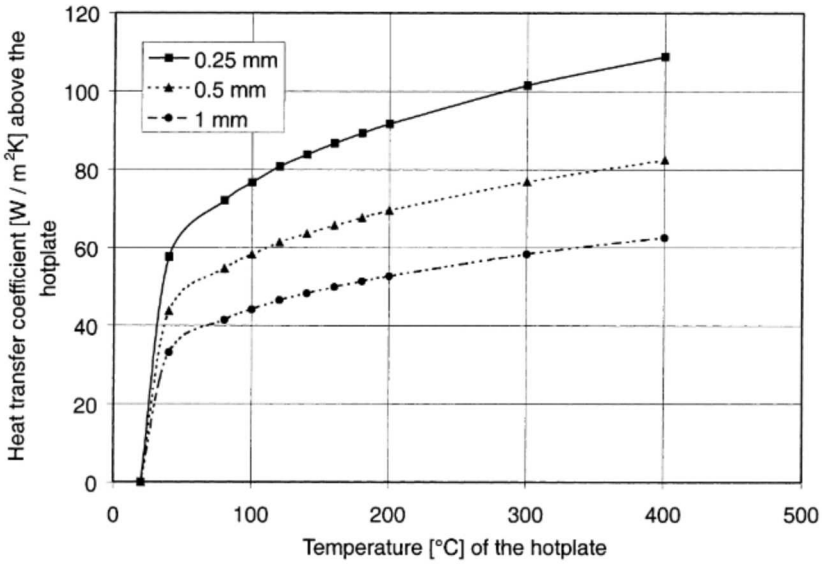

Fig. 13. Mean heat transfer coefficient for free convection above horizontal plates with edge lengths 0.25, 0.5 and 1 mm. Ambient temperature is set to 20°C.

rather questionable. Anyway, also the shown results should be considered just as an estimate as the used empirical equations are actually evaluated for much larger hotplate sizes. This fact and the variation of a_m with hotplate size and temperature might be the reason for the rather different values found for a_m in literature. For example, Astie et al. [32] use as heat transfer coefficients 125 W m^{-2} K^{-1} for the front side and 60 W m^{-2} K^{-1} for the backside of a closed membrane. Hille and Strack [27] suppose that the heat transfer from a closed membrane to the ambient is determined by convective heat transfer on the front side and by thermal conduction through the air on the backside and use a heat transfer coefficient of 30 W m^{-2} K^{-1} on the front and thermal conductivity of 30 mW m^{-1} K^{-1} at the backside.

With the help of calculated mean heat transfer coefficients, the total heat flow above a heated membrane can be easily calculated. Results are shown in Fig. 14. They demonstrate clearly, as expected, that power saving can be best done by minimization of heated membrane area and operation temperature.

2.2.1.3. Radiation. The expression for radiation in Eq. (1)

$$Q_{radiation} = G_{rad}\,\varepsilon\,(T_{hot}^4 - T_{amb}^4) \quad (14)$$

has been obtained with the assumption that the heated membrane area behaves like a gray emitter, i.e. the degree of emission of the heated membrane is set equal to the degree of absorption [31]. Under the assumption that the

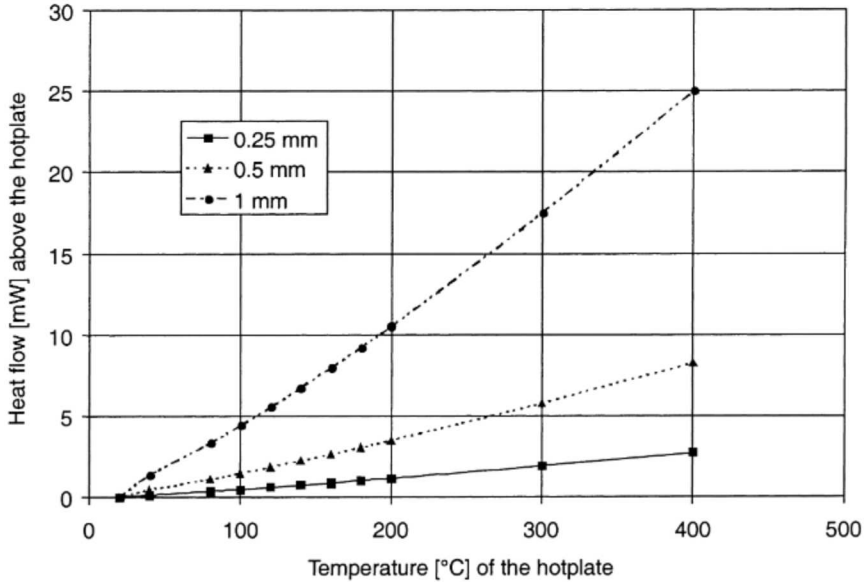

Fig. 14. Heat flow for free convection above horizontal plates with edge lengths 0.25, 0.5 and 1 mm. Ambient temperature is set to 20°C.

heated membrane area A radiates in all directions, the geometry factor G_{rad} can be set to $G_{rad} = 2A$. Heat losses due to radiation increase thus with heated membrane area. Generally the heat losses due to radiation amount only some percent of the total heat loss [11,16,27,32] but due to the T^4-dependency they should be considered with care if very high sensor operation temperatures are applied. However, one can reduce the radiation dramatically by coating the backside of the membrane with glossy materials like gold, as proposed by Müller et al. [29]. Gold or any other glossy materials have compared with silicon, $\varepsilon_{Si} = 0.2$–0.4, or silicon oxide, $\varepsilon_{SiO_2} = 0.7$–0.9, a much lower emissitivity, $\varepsilon_{Au} = 0.05$, and can thus prevent radiation. With respect to the total power consumption one has to have in mind that the gold coating reduces not only radiation but increases the heat conduction through the membrane as gold or other glossy materials are in general good thermal conductors. Coatings should therefore be chosen as thin as possible and only used in the heated membrane area to avoid an increase of the thermal conduction through the membrane.

2.2.1.4. Conclusions. The simple models, which were described in the last paragraphs, can give a feeling about the parameters influencing the heat losses of micromachined gas sensors. One can conclude that the total power consumption can be minimized by:

- constructing thin membranes consisting of materials of low thermal conductivity;
- use of suspension beams with high length-to-width ratio;
- adjusting the heater size (edge length a) to the size of the closed membrane (edge length b) as b:a = 3:1;
- decreasing the heated area;
- choosing a large pit depth of the suspended membrane;
- gold coating at the backside of the membrane.

Some actual values for power consumption of the different types of micromachined sensors are listed in Table 2. The power consumption of suspended membranes is, as predicted from simple models, in most cases smaller than those for closed membranes. An increase of membrane size for a fixed heater size leads to reduction of power consumption due to decreasing heat losses along the membrane. Despite of the large thickness of about 25–30 mm, the nitrided porous silicon-membrane shows a decent power consumption. This example illustrates the enormous influence of membrane material's thermal properties. The low thermal conductivity of the nitrided porous silicon can compensate for the membrane thickness.

Even though one can qualitatively argue with the simple models explained above, a quantitative determination of the total power consumption cannot be done by simple addition of the different heat losses as motivated in Eq. (1). The different heat losses interfere with each other. At each single volume element of the membrane one has to deal with heat conduction through the solid, heat losses to the air and radiation. To account for that numerical models as described in Section 2.2.4 have to be used.

In this whole discussion one should not forget that besides low power consumption the gas sensor's functionality and mechanical stability have to be maintained. For example, the heated active area which should be small with respect to power consumption needs to be large to enable the measurement of the in general highly resistive sensing materials. Only large active areas which allow for a high length-to-width ratio of the electrodes lead to reasonable small sensor resistances. Another example is the length-to-width ratio of suspension beams which cannot be increased arbitrarily without loss of mechanical stability and increase of current density along the metal lines needed for electrical connection [10].

2.2.2. Heater design: control of temperature distribution

The heater design is crucial for control of the temperature distribution along the active area. To achieve a desired temperature distribution one has to adapt heater and substrate geometry carefully. Silicon plugs or high thermal conducting films as presented in Section 2.1.2 may help to improve uniform temperature distributions [30]. In

Table 2
Thermal characteristics of micromachined gas sensors in comparison to a screen-printed ceramic sensor[a]

Type	Membrane edge length (mm)	Heater edge length (mm)	Temperature (°C)	Power consumption	Thermal time constant	Reference
Si_3N_4/SiO_2-membrane	1.7	900	500	130mW	10ms	[12]
	1–1.5	±	400	30mW	±	[15]
	0.8	500	450	230mW	±	[32]
	1.3	500	450	190mW	±	[32]
	1.8	500	450	160mW	±	[32]
NPS-membrane	1.5	±	400	170mW	56ms	[17]
Spider (anisotropic etch)	0.1	0.1	300	12mW	3ms	[18]
	0.1	0.1	350	20mW	0.2 ms	[10]
	0.1	0.1	320	40mW	2–5 ms	[23]
Spider (sacrifical etch)	0.1	0.1	200	15mW	±	[20]
Ceramic	±	±	330	1W	10s	[89]

[a]NPS = nitrided porous silicon.

general, predictions of temperature distribution are hardly obtained without extensive numerical calculations. Nevertheless, two different practical solutions are presented to illustrate how a uniform temperature distribution can be obtained.

First of all, it has to be pointed out that the heating of an active area with constant power per area, results not in a homogeneous temperature profile. In this case, the inner part of the heated area experiences heat losses only to the ambient air and radiation, whereas the outer part additionally suffers from heat losses through the membrane, respectively, the suspension beams. This causes the borders of the active area to be colder than the inner part. To compensate for that spatial varying heating power is needed.

Hille et al. [27] and Fung et al. [10] solve this problem by the use of an area heater and a ring heater. The ring heater serves thereby for compensation of the heat losses through the membrane such that heat flow through the membrane becomes zero inside the ring heater. One difficulty of this two-heater-approach is to determine the compensating heating power, i.e. to adjust the power of the heaters correctly.

Another approach is represented by Aigner et al. [38] and Guidi et al. [39]. They use a double-spiral with variable width [39], respectively, pitch [39], as heater structure. Aigner et al. varies the heater width with a factor 2.5 to obtain a uniform temperature distribution. Guidi et al. could achieve a reduction of the radial temperature gradient from about 5 K mm^{-1} for standard meander-shaped heaters to 0.2 K mm^{-1} for their double-spiral-shaped Pt-heater. A disadvantage compared with the two-heater-approach is that temperature homogeniety depends on design and cannot be adjusted later on.

2.2.3. Thermal transient response

A simple expression for the thermal transient response of the sensor can be obtained neglecting the actual temperature distribution inside the sensor and describing the thermal behavior just with one overall thermal resistance R_{therm} and one overall capacity C. Heat balance between heating power P_{el} and heat losses results in the expression

$$P_{el} = C\frac{dT}{dt} + \frac{T - T_{amb}}{R_{therm}} \quad (15)$$

This equation allows the calculation of the temperature response to an arbitrary heating power input; solutions can be found using Fourier and Laplace analysis. The temperature response to a step function is given by

$$T = T_{amb} + P_{el}R_{therm}\left(1 - e^{-t/\tau}\right) \quad \tau = R_{therm}C \quad (16)$$

As the so-obtained thermal time constant depends linearly on thermal resistance and capacity, a sensor with low thermal mass and small thermal resistance will show the fastest response. Due to the fact that a small thermal resistance leads not only to fast thermal response but also to an increase in power consumption, the choice of thermal resistance will be a trade-off between power consumption and fast thermal response. The thermal capacities of common sensor materials, listed in Table 1, differ scarcely. Minimization with respect to thermal capacity can thus only be achieved by reduction of heated mass, i.e. minimization of the sensor's active area and membrane thickness. It is therefore not surprising that the small suspended membranes show in general (values are listed in Table 2) faster transient response than the larger closed membranes.

Finally, it should be pointed out that the thermal time constant is in general temperature dependent. Sberveglieri et al. [12], for example, showed that the thermal time constant varies in the same way as the thermal resistance, both being effected by the temperature dependence of the thermal conductivity of air.

2.2.4. Thermal simulations [40]

Numerical approximations of the temperature distribution, the total heat loss and the transient response can be obtained by replacing the sensor by a set of points for which temperature as function of time is calculated. This set of points is called the computation grid or mesh. The right choice of the computational grid is very important to obtain good approximations. Increasing the number of node points results in better accuracy but leads at the same time to an increase of computational time. Therefore, it is often better to use a non-uniform grid which models the parts of the sensor which are subject to large changes with a narrow grid and regions with nearly no changes in temperature with a rather rough grid.

One way to derive the equations for the node temperatures is to divide the sensor into elements and apply the heat balance to each individual element. For each element a point, e.g. the center of the element, is selected as node. Temperature and thus flow variations over the element are neglected. The node temperature is considered to be representative of the entire element.

Another possibility is to start with the differential equation, which is the mathematical description of the heat balance of an infinitesimal element, and replace the differentials by finite differences expressed in terms of the node-point temperatures. This method is known as finite-difference method.

In either case one has to solve a set of equations relating the temperature at the nodes to each other. This might get rather complicated for a large set of nodes and boundary conditions. Anyway, a lot of analysis tools are nowadays available which can take over this study, e.g. solutions can be found by description of the thermal system by electrical equivalents and use of the many standard circuit analysis tools such as SPICE, or by advanced finite-element methods (FEM) such as ANSYS.

2.2.4.1. Electrical–thermal analogies.

Electrical–thermal analogies can be found as the behavior of the heat flow and temperature in thermal systems is described mathematically by the same equations as those used for

Table 3
Electrical–thermal analogies of some selected properties

Thermal property	Electrical property
Temperature: T (K)	Voltage V (V)
Heat flow, power: P (W)	Current: I (A)
Resistance: R (K W^{-1})	Resistance: R (Ω)
Capacity: C (J K^{-1})	Capacitance: C (F)
Thermal conductivity: l (W m^{-1} K^{-1})	Electrical conductivity: s (Ω^{-1} m^{-1})

electrical currents and voltages in electrical systems. A list of some analogies can be found in Table 3. By using those analogies, the membrane of a micromachined gas sensor can, for example, be modeled as sketched in Fig. 15. A uniform grid is applied to describe the membrane of thickness d. The node (i, j) is heated up to a temperature T above ambient temperature T_{amb} by electrical power P_{el}, heat flow takes place along the membrane through the thermal resistances R_{therm} and through the ambient R_{air}, the transient response depends thereby on the thermal capacity C of the element (i, j). The advantage of such models is that the sensor's thermal as well as electrical behavior can be modeled with the same analysis tool. On the other hand, the flexibility of FEM tools cannot be reached.

2.2.4.2. Finite element method. FEM describes the solution on a given geometry (which may be one-, two- or three-dimensional) by means of a finite number of (line, surface or volume) elements. These can be chosen rather arbitrarily. FEM can account for complicated boundary conditions and temperature-dependent thermal properties, e.g. temperature-dependent thermal conductivity of air. The node equations can thus become rather complicated. Finite-element methods are therefore available in the form of complete software packages, which include facilities for mesh generation, element definition and equation solving.

2.3. Mechanical design

Micromachined gas sensors are not only a challenge with respect to thermal design but also with respect to mechanical design. Only by choosing the right mechanical design the following typical mistakes can be avoided:

- large intrinsic or thermal-induced membrane stress leading to membrane deformation/breaking of the membrane;
- plastic deformation at the metal–SnO_2 contact area;
- deformation/breaking of the membrane due to deposition of sensing layer;
- stress in the metallization sandwich structure;
- thermometer-resistance shift due to mechanical and thermal stresses.

To avoid these failures, the right set of process parameters have to be found and the processes need to be well-controlled. Very often one will have to rely on trial and error, as thin film mechanical properties depend strongly on microstructural characteristics like: grain size, orientation, density, stochiometry. These properties are determined by specific deposition conditions. Additionally, the film microstructure changes with heat cycles. The result can be the drift of the mechanical characteristics but also the possibility to adjust the layer's properties by annealing steps.

Intrinsic stress in single layers or multilayer compositions can occur due to thermal stress and residual stress [41]. Thermal induced stress is caused by mismatch in the thermal expansion coefficients of different films, which might lead to undesirable bimettalic warping effects, or it is caused by non-uniform temperature distribution which might even vary in time. The latter points out that thermal design and mechanical design are strongly tied up with each other. Residual stresses can be led back to the fact that thin films as-deposited are not in the most favorable energetic configuration resulting in compressive or tensile stress.

Residual stresses are generally much larger than thermal stress [41] and the control of residual stress of single layers

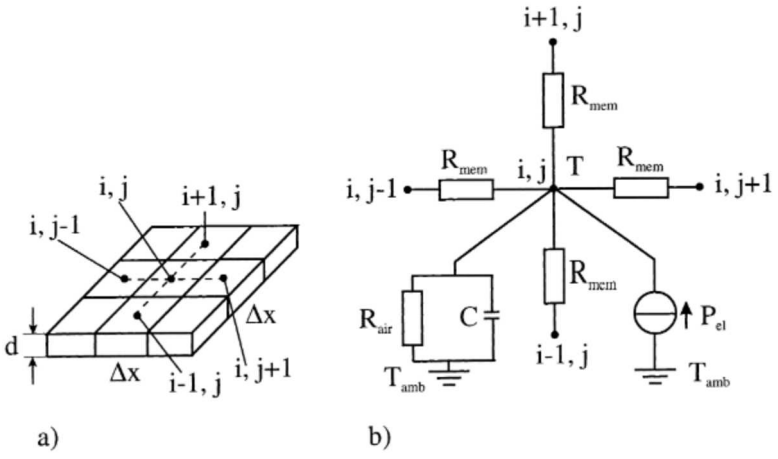

Fig. 15. Multi-element model of a membrane: (a) element definition; (b) equivalent circuit.

Table 4
Residual stress in thin films

	SiO_2	Si_3N_4	$SiN_{1:2}$	Reference
Stress (GPa)	±1 ±0.27	1.2	± ±0.6	[41] [43]

and especially of multilayer systems seems to be crucial for membrane stability [42]. The resultant residual stress, s_r, of a stacked membrane can be approximated by

$$s_r \approx \frac{s_1 d_1 + s_2 d_2 + \cdots}{d_1 + d_2 + \cdots} \approx \frac{\sum_{i=1}^{n} s_i d_i}{\sum_{i=1}^{n} d_i} \quad (17)$$

where d_i and s_i are thickness and intrinsic stress of the different membrane layers. Rossi et al. [43] suggests an acceptable range for resultant residual stresses as $-0.1\,\mathrm{GPa} < s < 0.1\,\mathrm{GPa}$.

To obtain such low residual stress in single layers is difficult. Frequently used materials like silicon oxide and silicon nitride show, as listed in Table 4, large compressive, respectively tensile stress. But right combination of those materials can lead to acceptable resultant residual stress. In this context it should be pointed out that simple addition of residual stress of single layers as suggested in Eq. (17) and simulation of the membrane stress by e.g. FEM simulations is not always possible. The properties of a single layer i might change under annealing and processing of subsequent layers thus leading to different stress of layer i in the multilayer system than in the single layer. Therefore, one often depends on experimental measurement of residual stress to design a membrane with low intrinsic stress. As experimental techniques, one can use, e.g. curvature measurements of the whole wafer, in situ stress diagnostic structures like doubly supported beams or Guckel rings, which rely on warping or buckling [41]. Such an experimental control is not only of interest for the design of new sensors but also as process control to guarantee reproducible film structures. Reproducibility of film structures and thus mechanical as well as thermal properties is crucial for sensor production.

A simple practical measure for the mechanical stability of micromachined gas sensors is the production yield [25,30]. More realistic pictures with respect to mechanical stability under normal sensor operation can be obtained by long-term reliability tests. Guidi et al. [39] uses for example a 10-day test pulsing the sensor between 200 and 500°C each 2 s to confirm mechanical stability. Heating of the sensor is thereby very important as the various films in the membrane stack expand thermally leading to additional compressive stress. A mechanical stability check should therefore always be performed under actual operation temperatures.

Low et al. [42] even point out that not only the actual temperature of a sensor has an influence on mechanical properties but also the temperature ramp-up rate. They argue that a fast temperature ramp-up may cause the membrane to rupture due to excessive stress changes and look at thermal induced stress as function of heating algorithms.

Another approach is given by Bosc et al. [44]. They developed an accelerated life testing algorithm to model 3 years of real life of micro-machined chemical sensor in about 3 weeks. The normal operation of their devices is 5 s at 400°C and 10 s at 100°C. They increased the cycle-frequency to 0.1 s at 400°C and 0.2 s at 100°C, i.e. a frequency where the sensor still can reach the thermal and mechanical steady-state of normal operation and thus the same mechanical deformations as in normal mode. They suppose that the failure processes which arise from the dynamic effects are thereby reproduced accurately. Their interest were especially in the drifts of heater and sensor resistances over life-time and their results proof that their fixed drift limits of heater resistance ±10% and of the sensor resistance ±35% could be reached.

Finally, one should notice that not only the mechanical properties of the thin film layers influence the stability of the micro-machined sensors but also the macroscopic dimensions. Decrease of the lateral dimensions and increase of the thickness of the membrane and suspension beams can lead to much higher stabilities. But at the same time as stability is improved the thermal losses are increased as shown in Section 2.2.1. The choice of membrane dimensions is therefore a trade-off between high-mechanical strength and small thermal heat losses.

3. Sensitive layer

3.1. Formation of tin oxide layer

The deposition of the sensing layer is the most crucial part in the preparation of gas sensors. Normally the deposition is carried out as the last process step in the fabrication of a micromachined gas sensor. This way poisoning of standard equipment with tin oxide can be avoided and the gas sensing film can be protected from uncontrollable modifications during later process steps. Some possible deposition techniques are listed in Table 5. Whereas the various chemical and physical vapor deposition techniques are mostly standard processes in semiconductor industry the liquid deposition techniques are rather uncommon. However, the compatibility of the latter, i.e. screen-printing [17] and drop deposition techniques [30], with semiconductor processes have been proven feasible. The main difference between screen-printed or drop deposited films and CVD or PVD films occurs due to their different film thickness. Whereas the former, the so-called thick films, posses layer thickness of several microns, the layer thickness of the latter, the so-called thin films, varies between 20 and 1000 nm. Beyond this classification in thin and thick film sensors the various deposition techniques lead to sensing films of different microstructure. Some examples are given in Figs. 16–18

Table 5
Deposition techniques used for the preparation of metal oxides such as SnO_2 [90][a]

Paste/slurry deposition	Chemical vapor deposition (CVD)	Physical vapor deposition (PVD)	
		Sputtering	Evaporation
Screen-printing	Thermal CVD	Sputtering	Molecular beam epitaxy
Drop deposition	Plasma activated CVD	Reactive sputtering	Thermal evaporation
Dip coating	Laser induced CVD	Cathode sputtering	Reactive evaporation
Spray deposition	Electroless plating	With bias voltage	Ion plating
			Reactive ion plating
			Arc evaporation
			Laser evaporation

[a]Liquids are formed by a mixture of inorganic additives, organic binders and metal oxide powders. The metal oxide powders are thereby prepared either by sol–gel from precursors, precipitation of precursors, or laser pyrolysis. Details can be found in [91].

3.2. Mechanical and thermal properties of the sensing layer

The sensing film influences the mechanical and thermal properties of a micromachined gas sensor. The effect of the sensing film depends strongly on whether thin or thick films are used. Exact data on the interaction between micromachined substrate and sensing film are not available, but one can argue as follows: thin sensing films can lead to additional stress in the membrane stack if the intrinsic stress of the sensing film is not well-adjusted to the different membrane layers whereas the deposition of thick sensing films comes along with the introduction of a large mass of sensing material which has to be carried by a rather thin membrane. Mechanical robustness of a micromachined gas sensor requires, therefore, for thin films low-stress deposition of the sensing layer and for thick films high mechanical strength of the membrane under the high load of a thick sensing film.

Table 6
Thermal conductivity and capacity of SnO_2 after [92]

Thermal conductivity ($W\,m^{-1}\,K^{-1}$)	Thermal capacity ($10^6\,J\,m^{-3}\,K^{-1}$)
28.5–30.6	2.6

Comparison of the thermal properties of SnO_2 listed in Table 6 with those of standard membrane materials listed in Table 1 shows that the thermal conductivity of SnO_2 is somewhat larger than that of standard membrane materials whereas the thermal capacity of SnO_2 is comparable to the latter. For thin film sensors, whose sensing film thickness is much smaller than the total membrane thickness one expects, therefore, only a small increase in thermal conductivity and thermal mass in comparison to a bare sensor substrate. Power consumption and thermal response time of thin film sensors is thus not strongly influenced by the thin

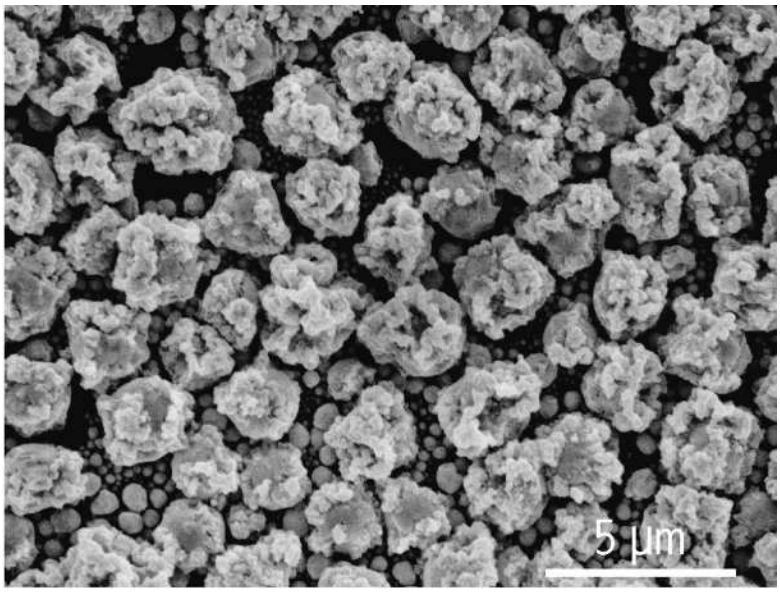

Fig. 16. SEM image of a thin film SnO_2-layer deposited by a technique called rheotoxial growth and thermal oxidation (RGTO). A detailed description of this technique can be found in [90].

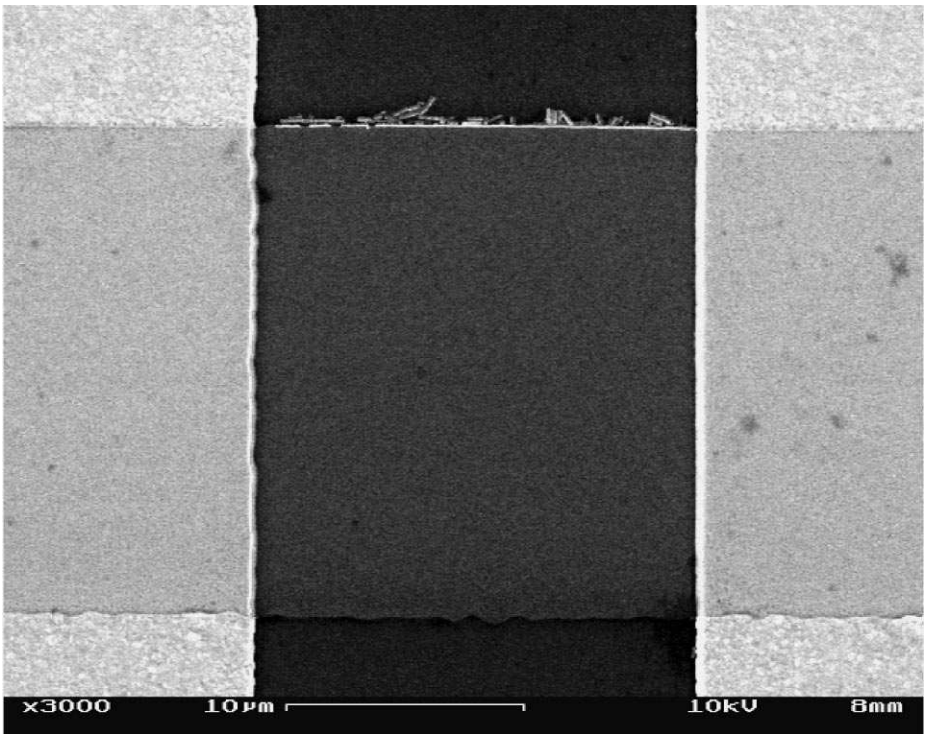

Fig. 17. Sputtered thin film [96].

sensing film. That is different for thick film sensors with film thickness comparable to membrane thickness. In this case the sensing film introduces a large extra thermal mass which leads to an increased thermal time constant. Beyond that the larger thermal conductivity in the active region leads to a smoothing of the temperature profile over the active area and an increase in power consumption due to additional heat losses through the membrane.

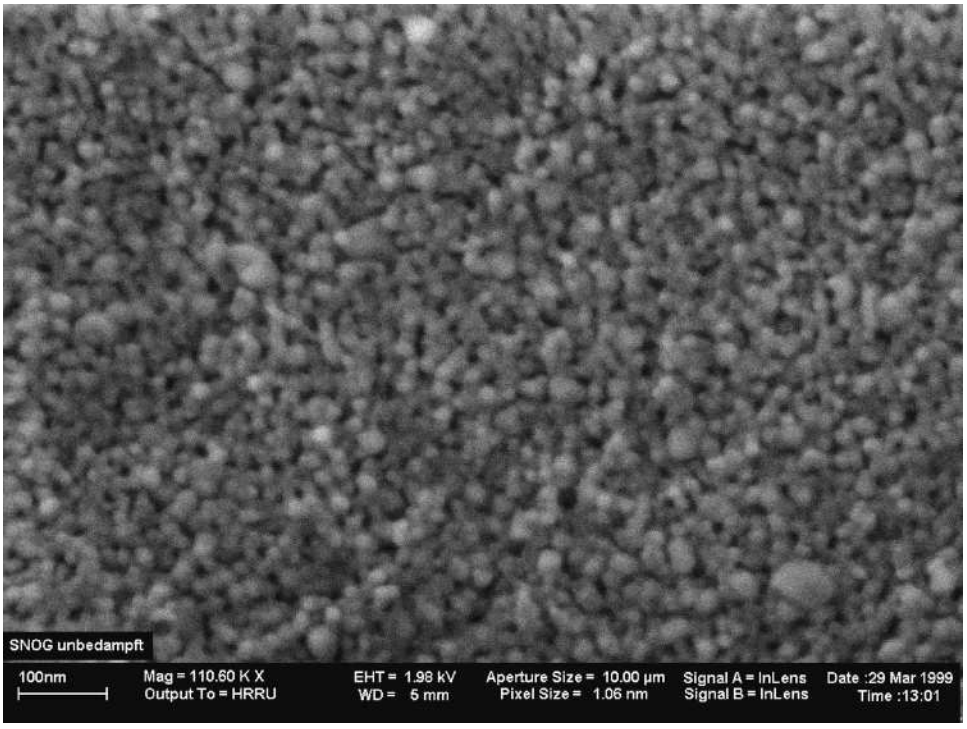

Fig. 18. SEM picture of a thick sensitive layer obtained by screen-printing at IPC.

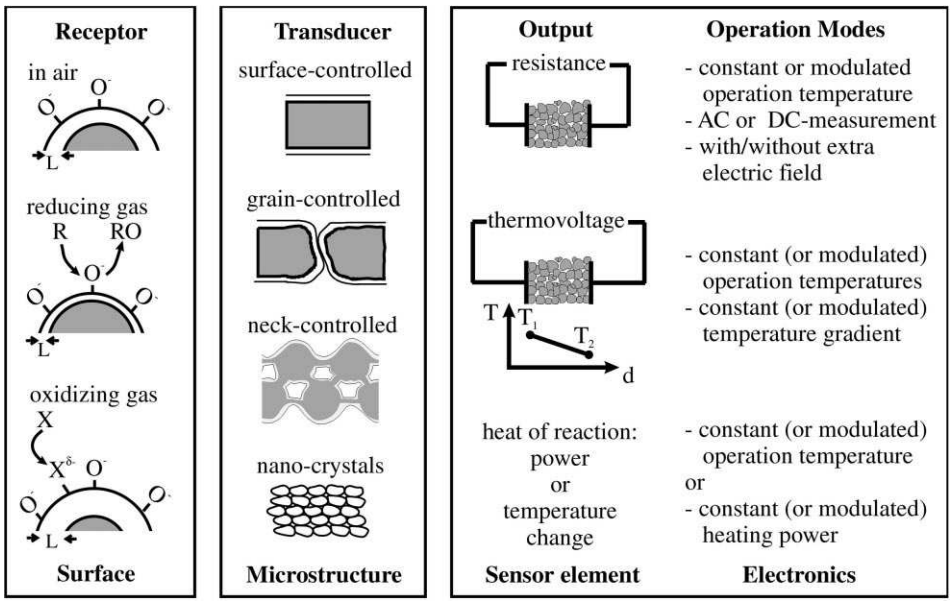

Fig. 19. Schematic view of gas sensing. The receptor, i.e. the semiconductor surface, reacts under exposure to reducing or oxidizing gases with decrease respectively increase of the electron depleted surface region. L denotes thereby the thickness of the depletion layer. The gas-induced changes at the semiconductor surface are transduced by the transducer, i.e. the microstructure of the sensing material, into an electric output signal. The grain size and different grain intersections have thereby a strong influence on the final output signal [5]. In most cases the sensor resistance is monitored as output signal but thermovoltages or changes in sensor temperature (constant power operation), respectively, heating power changes (constant temperature operation) due to gas-specific heat of reactions at the surface can also be used. The possible operation modes are manifold and allow manipulation of sensor properties.

From this short argumentation one can conclude that the knowledge about the various interactions between sensor substrate and sensing film and their influence on sensor characteristics is crucial to design a sensor with high mechanical stability, low power consumption and fast thermal response.

4. Gas sensing: receptor, transducer and operation modes

The actual gas sensing consists of three different parts: receptor, transducer and operation mode. These parts are presented in Fig. 19. For details one might refer to [45–52]. In this context only a short description of microstructures is given to demonstrate the different transducer function of thin film versus thick film sensing layers. The former are frequently used for micromachined gas sensors whereas the later are applied to ceramic gas sensors and some of the micromachined sensors. Opportunities to improve sensor performance by appropriate choice of output signal [5] and operation mode [5] are presented. Already with one single sensor one has plenty of possibilities to obtain not only one-dimensional but multi-dimensional output information. The use of several output signals instead of one, e.g. simultaneous measurement of sensor resistance and thermovoltage, or the use of modulated operation temperature instead of constant operation temperature are some of those discussed in the following.

4.1. Microstructures

A lot of different microstructures are known, some are presented in Figs. 16–19. The microstructures depend strongly on the choice of deposition technique. Beyond that the addition of dopants, promoters as well as the chosen burnig-in-cycles have an impact on microstructure and sensing properties. The microstructure together with the chosen operation mode determines how the recognition of a gas at the sensor surface is transduced in one or several output signals. Most of the CVD and PVD deposition techniques applied to micromachined gas sensors lead to microstructures and transducer functions which are very different from the one obtained by thick film deposition. Bârsan et al. [53] outline the differences as follows. They make a simple distinction between two types of layers, compact and porous layers. The former one is obtained by most CVD and PVD techniques and the latter is characteristic for thick film deposition techniques and RGTO[3]. The geometry and the band bending of theses two microstructures is presented in Fig. 20.

The interaction of compact and porous layer with surrounding gases is rather different. Porous layers are accessible to gases in the whole volume whereas compact layers only interact with gases at the geometric surface. The gas-active surface of porous layers is therefore much larger than in case of compact layers. Additionally, the two layers differ in the way how gas-induced changes at the gas-active

[3] Rheotaxial growth and thermal oxidation of tin layers

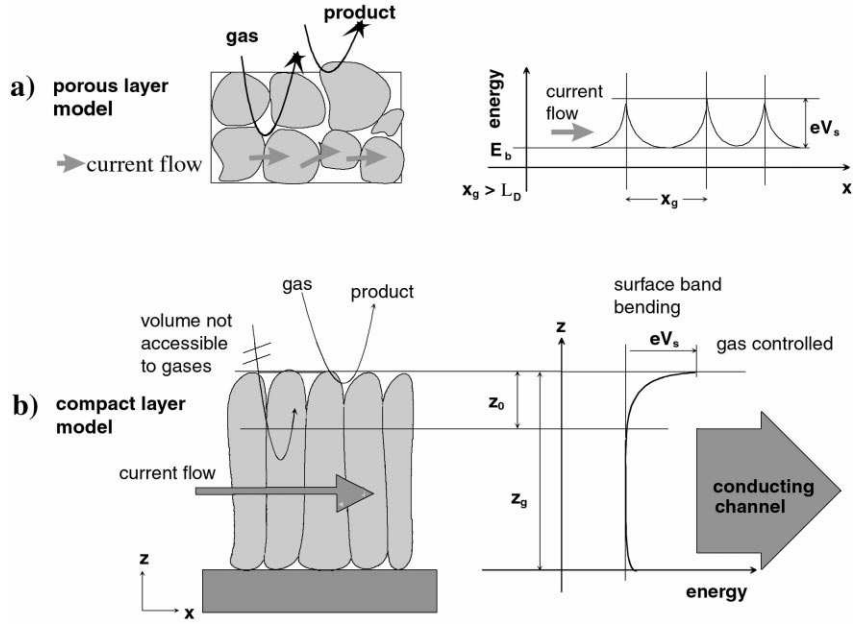

Fig. 20. Schematic representation of (a) porous and (b) compact sensing layer with geometry and energy band. x_g grain size, L_D Debye length, eV_s band bending, z_0 thickness of the depleted surface layer and z_g layer thickness.

surface are transduced in a sensor output signal such as sensor resistance: in case of a compact layer current flows through two resistances put in parallel, one being equivalent to the geometric surface which is affected by gas reactions, the other corresponding to the gas-unaffected bulk. The sensitivity of compact layers depends, therefore, strongly on the layer thickness: only in case that the thickness of the electron depleted surface thickness is about the size of the compact layer high gas sensitivity can be expected. A small gas concentration can then work like a switch closing or opening the conducting channel. In case of porous layers the situation is different, each grain possess a surface depleted area and current has to pass through the intergranular contacts, the resistances of gas-unaffected bulk and surface-depleted areas are put in series.

These two models, even though simplifying the real microstructures of gas sensors, show that the expected sensor characteristics of most thin film sensors are expected to behave differently from thick film sensors. Due to the larger gas-active surface area of porous layers compared to compact layers higher sensitivity and immunity to poisoning and thus altering of sensors is expected in case of porous layers. This fact might be a strong argument for the trials to manufacture micromachined substrates which are compatible with thick-film deposition techniques and the search for thin film deposition techniques such as RGTO which result in porous layers.

4.2. Resistance measurements

The sensor resistance is the best-known sensor output signal and is in most cases determined at constant operation temperature and by DC-measurement. AC-measurements have also been reported [54] but are more frequently used in impedance spectroscopy [45] at a modeling level. The sensor properties such as gas sensitivity, selectivity and stability, depend strongly on operating temperature and the semiconductor microstructure as discussed above, but can also be influenced by electrode material [55] and electrode geometry [56,57].

Tables 7 and 8 represent several sensor signals obtained by thin and thick film gas sensors. CO and NO_2 have thereby depicted as examples for reducing, respectively, oxidizing gases and the sensor signals are defined as $S_{CO} = R_{air}/R_{CO}$, respectively, $S_{NO_2} = R_{NO_2}/R_{air}$ with R_{air} denoting the sensor resistance in air without CO and NO_2, and R_{CO}, respectively, R_{NO_2} the sensor resistance with CO, respectively, NO_2. In literature, the so-defined sensor signals are sometimes used as a measure for sensor sensitivity. The examples show that thick film sensors in general posses better response to reducing gases than thin film sensors whereas in case of oxidizing gases the sensor signals are about the same.

An example for the influence of operating temperature and electrode material is given in Fig. 21 in case of exposure to CO. Such kind of relations between operating temperature, electrode and sensor material and sensor properties have been intensively explored in the last years and applied to sensor arrays but nevertheless one has still to bother with distorting cross sensitivities, long response times and bad long-term stability. To overcome these difficulties micromachined gas sensors either with new-type of electrode configuration, electric fields applied to the sensing film, or modulated operation temperature offer new possibilities.

Table 7
CO sensor signals of various thick and thin film sensors[a]

Sensor type	CO concentration (ppm)	CO sensor signals	Reference
Thick film sensors			
TGS 2201 thick film ceramic sensor	10–100	1.7–3.3	[93]
Taguchi-type from IPC	50	9	[94]
Screen-printed thick-film ceramic sensor from IPC	50	10	[94]
Different microstructured sensors with drop deposited thick film from IPC	50	8, 21, 40	[94]
Thin film sensors			
MGS1100 from Motorola, RGTO thin film on micromachined substrate	10–1000	1.05–11	[74]
Micromachined sensor with RGTO thin film	10–100	1.1–2	[66]
Thermally activated, CVD-deposited thin film on micromachined substrate	5–45	1.05–1.6	[23]
Micromachined sensor with 60 nm thick sputtered thin film	50	1.3	[94]

[a]Data values are obtained under constant operation temperature except for the Motorola sensor which is temperature pulsed due to the manufacture's proposed operating conditions.

Table 8
NO_2 sensor signals of various thick and thin film sensors

Sensor type	NO_2 concentration (ppm)	NO_2 Sensor signals	Reference
Thick film sensors			
TGS 2201 thick film ceramic sensor	0.1–1	1.5–10	[93]
Screen-printed thick-film ceramic sensor from Bosch	1–5	1.4–2.9	[89]
Screen-printed thick-film ceramic sensor optimized for NO_2-detection	0.2–5	40–200	[91]
Thin film sensors			
25 nm thick sputtered thin film	1–5	4–11	[62]
Micromachined sensor with RGTO thin film	0.25–5	6–20	[66]
60 nm sputtered thin film	5–50	2–4	[60]
60 nm sputtered thin film with electrode configuration featuring a JFET-like transducer mechanism	0.01–1	2–100	[58]

4.2.1. Electrode configurations

In the following an electrode configuration is presented which leads to a thin film gas sensor being highly sensitive to oxidizing gases like NO_2. Approaches to increase the – compared with thick films – very low sensitivities of thin films to reducing gases like CO have not been found in literature up to now.

Hoefer et al. [58] uses a highly asymmetric electrode configuration which allows the attainment of NO_2-sensor signals as high as 2–100 for NO_2-concentrations between 10 ppb and 1 ppm. One electrode is thereby realized with a large contact area and antimony-doping of the adjacent 60 nm thin SnO_2-film resulting in an Ohmic contact to the sensing film, the other electrode consists of a very small contact area building up a Schottky-contact to the adjacent SnO_2. The 60 nm thick SnO_2-layer is supposed to behave like a compressed layer such that the sensor conductance is mainly determined by the width of the conductive channel in the middle of the layer. The boundaries of this channel are given by the surface depleted region and the depletion layer at the Schottky-contact. By application of a forward-biased voltage at the Schottky contact one expects a reduction of the channel width such that the exposure with oxidizing gases, e.g. NO_2, lead to a quenching of the channel resulting in a large increase of sensor resistance and thus improved sensor signal. Such a behavior is reported for a forward bias of 2 V and results not only in a very NO_2-sensitive device but also a high selectivity: to counterbalance the effect of 10 ppb NO_2 100 ppm CO are necessary.

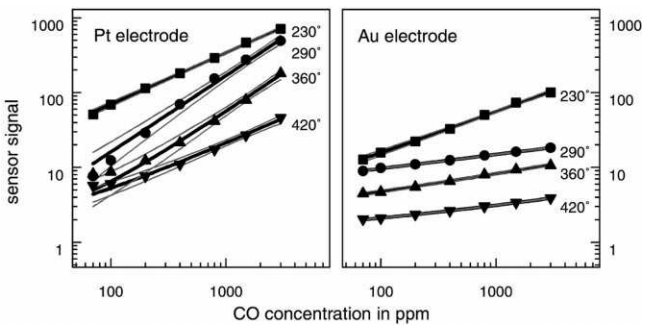

Fig. 21. Result from [74] on Pt-doped thick film sensors optimized for CO detection. The sensor signal is $S_{CO} = R_{air}/R_{CO}$ with R_{air} and R_{CO} denoting the sensor resistance in air without respectively with CO.

This and further examples [59,60] show that already the variation of electrode configurations can be used to modify the sensing properties of thin film sensors. This offers the chance to improve the selectivity of a single sensor or to built up sensor arrays consisting of individual thin film sensors of the same material which differ only in electrode design resulting in even better selectivity.

4.2.2. Application of electric fields

Another possibility to modify sensing properties is achieved by electrode-heater configurations which allow the generation of electric fields perpendicular to thin sensing films. Hellmich et al. [61] uses a micromachined sensor with a Pt-heater and a 300 nm thick RGTO-SnO_2 sensing layer which are separated by a 700 nm thick SiO_2 insulation layer. By application and variation of a bias voltage between the heater and the sensing layer they obtain an electric field and achieve electron enhancement (positive bias voltage) or electron depletion (negative bias voltage) in the SnO_2-films thus leading to an alteration of the sensor signal.

Hausner et al. [62] built a similar device on a silicon substrate (not micromachined) consisting of a thin film SnO_2-layer separated from a polysilicon heater by an isolation layer of 1 mm thickness. Their device posses besides bottom electrodes located below the sensing film, top electrodes deposited on top of the sensing film. They obtain an electric field by use of a bias voltage between top electrode and heater and measure sensor resistance with the bottom electrodes. They report an increase of sensor resistance and sensor signal to NO_2 in case that a positive potential is applied to the top electrode. Beyond that the additional top electrode enables various measurement methods. Diffusion and surface effects can be separated by resistive measurement with the top electrode, the bottom electrode, and from top to bottom electrode [13].

4.2.3. Temperature modulations

Whereas the above presented electrode configurations and applications of electric fields are all used in context with thin film sensing layers and are rather new, temperature modulated operation of gas sensors has its roots already in the 1970s and were first applied for selectivity improvement of thick film ceramic sensors [63,64]. However, the large thermal response times of ceramic sensors probably prohibited the frequent use of temperature modulation techniques. First lately, with the availability of micromachined gas sensors of fast thermal response, temperature modulated operation became more and more a standard technique which is capable to improve selectivity [14], sensitivity [65] and reduce heating power [19,66]. A good summary about the early and latest approaches can be found in [67,68].

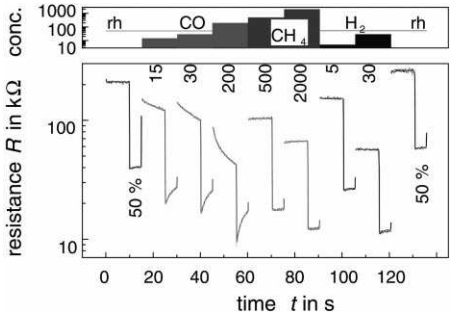

Fig. 22. Results from [74]: response curves of pulsed sensors to 15, 30, 200 CO; 500, 2000 methane and 5, 30 ppm hydrogen all obtained in 50% RH humidified air. The pulse mode was 10 s at about 350 °C and 5 s at about 490 °C.

The idea beyond temperature modulations is to take advantage of the temperature dependent conductance of metal oxide gas sensors and the temperature dependent kinetics of adsorption and desorption of gas molecules at the sensor surface. At the receptor, the gas-sensitive surface, temperature modulated operation leads to a modulation of the concentration of the adsorbed oxygen species and influences thus the reaction schemes and rates of incoming gas species. One can thus obtain time-dependent gas-specific signal patterns. For illustration, two examples, one for temperature pulsing, the other for temperature modulation through oscillation are depicted in Figs. 22 and 23,

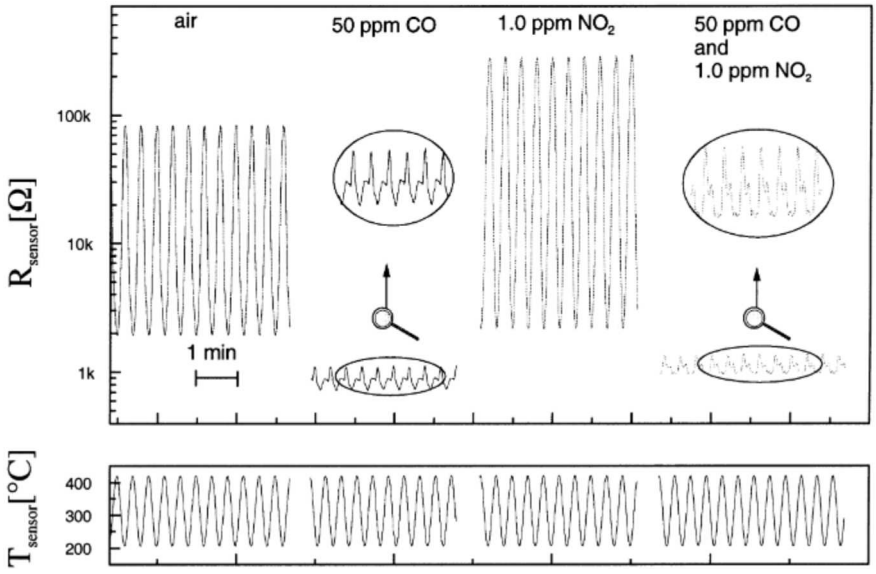

Fig. 23. Results from [72] on sinusoidal temperature modulations of a micromachined thick film sensor in synthetic air (50% RH) and during exposure to 50 ppm CO, 1.0 ppm NO_2 and a mixture of 50 ppm CO and 1.0 ppm NO_2.

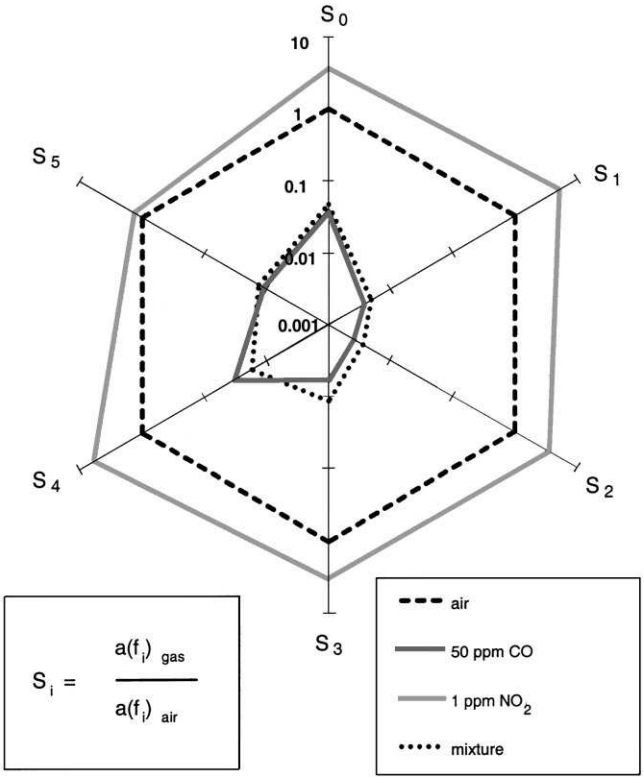

Fig. 24. Results from [72]. Polar plot representation of a fast Fourier transformation of the sensor signal shown in Fig. 23. The amplitudes of the fundamental frequency and of the first five harmonics are used as coordinates in the polar plot. Their values are normalized to the values in air and plotted in the figure for synthetic air (50% RH), 50 ppm CO, 1 ppm NO_2 and a mixture of 50 ppm CO and 1 ppm NO_2.

respectively. The differences in shape of the response curves upon exposure of different gases can clearly recognized. To optimize such gas-specific response curves one must in general vary empirically pulsing respectively cycling times as well as temperature ranges. A methodology for such empirical search can be found in [69–71].

To evaluate the rather complex signals different feature extraction techniques have been developed including various algorithms [67], fast Fourier transformation (FFT) with [72] or without neural network [73] and wavelet networks [69,70]. The so-obtained sensor results are with respect to sensor selectivity and sensitivity very promising, an example is given in Fig. 24.

The different temperature modulation techniques can in principal be applied equally well to ceramic sensors and micromachined sensors. The advantage of micromachined sensors is that cycling times and thus detection times can be chosen shorter. However, whether one can use temperature cycling times of only some milliseconds, which is possible with respect to thermal response, and still achieve gas characteristic signal patterns is rather questionable as the chemical response of the sensitive layer is in comparison with the thermal response slow [74]. This is due to the fact that gas specific patterns are mainly accomplished by the gas species characteristic interactions with surface oxygen species, which adapt only slowly to a certain temperature.

4.3. Thermovoltage measurements – Seebeck effect

A non-standard sensor output signal is the thermovoltage. Thermovoltage – often also called Seebeck voltage – is generated in case of a non-uniform temperature distribution across the sensing layer. Connecting electrodes to different temperature regions of such a sensing layer the Seebeck voltage V_S can easily be measured

$$V_S = a_S \Delta T \quad (18)$$

The Seebeck voltage is proportional to the temperature difference of the electrodes and proportional to the material-dependent and thus gas-sensitive Seebeck coefficient a_S of the sensing layer.[4] The so-obtained transducer is in contrast to utilization of resistive changes an active one. One can distinguish two different sensor types. They differ in the way how the temperature gradient across the sensing layer is generated.

Sensor type 1 posses a heater structure that allows the generation of a well-defined temperature gradient across the sensing layer and posses two electrodes for measurement of the gas-dependent Seebeck effect [75,76]. To operate such a sensor it is crucial to keep the temperature difference of the electrodes constant as otherwise not only the gas-dependent change of the Seebeck coefficient but also temperature changes are monitored by Seebeck voltage measurements. Results obtained with such sensors show that the thermovoltage is a linear function of the logarithm of the gas concentration [75] and can be related to the sensor resistance R_S [76] as

$$V_S = A + B \ln R_S \quad (19)$$

These experimental results are in-line with simple theoretical models used by Miszei [77] and Šetkový [75]. At a first glimpse one expects, therefore, that the measurement of Seebeck voltage offers no other information about surrounding gases as can be obtained by sensor resistance measurements. But by actual comparison as depicted in Fig. 25 one discovers that the combination of Seebeck and resistive measurements can yield additional information about the surrounding gases resulting in an improved sensor selectivity. The coefficients A and B seem to be gas-specific.

Sensor type 2 makes use of the catalytic effect of combustible gases to generate a temperature gradient across the sensing layer. For this purpose one part of the metal oxide surface is treated with a catalyst while the remainder of the metal oxide surface is untreated. In presence of combustible gases the reactions at the catalyst-treated surface are

[4] More exact one would have to write $V_S = a_S - a_M \Delta T$ with a_M the Seebeck coefficient of the metal contacting the sensing layer. But due to the fact that the Seebeck coefficient of metals is about an order of 100 smaller than that of the sensing semiconductor, a_M can be neglected.

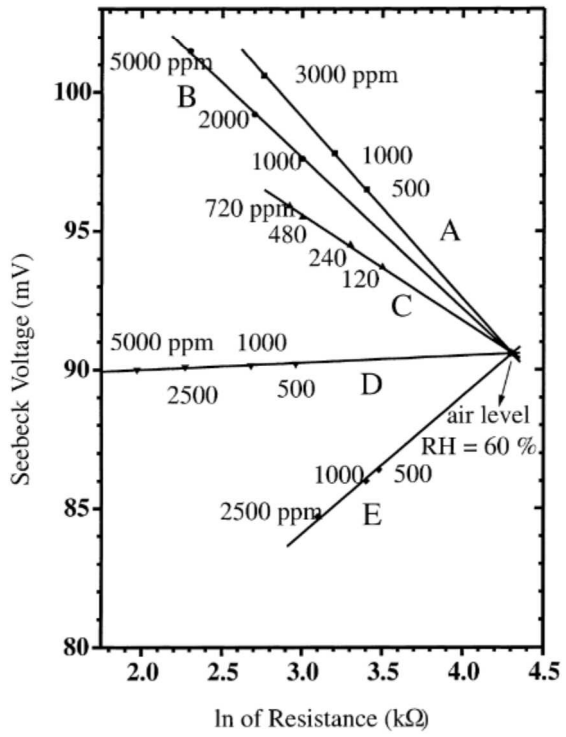

Fig. 25. Picture from [76] showing the possibility for discrimination of methane to propane by combination of Seebeck and resistance measurements. Line A, ethanol and acetone; line B, hydrogen; line C, carbon monoxide; line D, propane; line E, methane.

enhanced compared to the untreated surface and lead to a local temperature rise and thus to a thermovoltage between catalyst-treated and untreated part of the surface. This thermovoltage can be measured by electrodes positioned in the two different sensor areas [78] and can be additionally modulated by an electric ®eld [79]. The so-obtained sensor signal is a combination of gas-induced changes of the Seebeck coef®cient and temperature changes due to catalytic reactions in the presence of combustible gases. A clear separation between temperature changes and changes in material properties with this device is impossible. That is a disadvantage of this approach, especially if one tries to obtain a basic understanding of sensor reactions at the surface. A more appropriate approach supplying similar or even more information might, therefore, be obtained by simultaneous but separate measurement of temperature and resistive changes as discussed in Section 4.4.

From the above discussion one can conclude that thermovoltage can be used as an appropriate sensor output signal. Beyond that and that is the very interesting point about the Seebeck effect, thermovoltage measurements offer together with resistance measurements the possibility for improved sensor performance as presented in Fig. 25. A single sensor element operated with these two transducers modes, i.e. resistive and thermoelectric, might therefore be an alternative to sensor arrays or to temperature modulation techniques. However, a disadvantage in comparison with solely resistance measurements occurs due to the fact that the demands on temperature control circuitry are higher. Whereas a small change (some degrees) in absolute temperature modi®es the sensor material properties and thus the sensor resistance only slightly, a small variation of the temperature difference enters directly into the thermovoltage and can lead, e.g. to an error of 5% for a deviation of only 1 K from a ®xed temperature difference of 20 K.

So far, thermovoltage measurements have only been carried out with ceramic sensors. But due to the fact that temperature gradients can easily be achieved and controlled with micromachined gas sensors, Seebeck effect can also be measured with micromachined gas sensors.

4.4. Temperature changes Ð pellistor effect

The monitoring of temperature changes at catalytic surfaces, i.e. the measurement of the heat of reaction occurring by combustion of reducing gases with atmospheric oxygen at a catalytic surface, is well-known as gas sensing principle. Commercial available devices consist in general of an alumina pellet covered with a thick ®lm catalyst, mostly being a precious metal, and an embedded platinum coil which is used as heater and temperature sensor. A schematic view is given in Fig. 26. These devices are known as ``pellistors'' or ``calorimetric gas sensors'' [80].

The catalytic effect of metal oxides stays far behind that of precious metals. Metal oxide materials are, therefore, not appropriate to replace catalyst materials of calorimetric sensors. However, one can ®nd several approaches which apply pellistor techniques to metal oxides.

A device called semistor (semiconductor-based pellistor) uses the same structure as a pellistor except that the alumina and catalyst material is replaced by a metal oxide, such as tin dioxide. Even though the structure of such a device is that of a pellistor, gas-induced response, i.e. change in Pt-coil resistance, is rather caused by resistance changes of the metal oxide than by catalytic reactions. This is due to the fact that the metal oxide partially short-circuits the turns of the supporting Pt-coil. A reducing gas leading to a large drop in metal oxide resistance causes thus a drop in the Pt-coil resistance. Such one-electrode devices were frequently used in the former USSR. More technical details about such a device can be found in [81]. The semistor with its all-in-one-

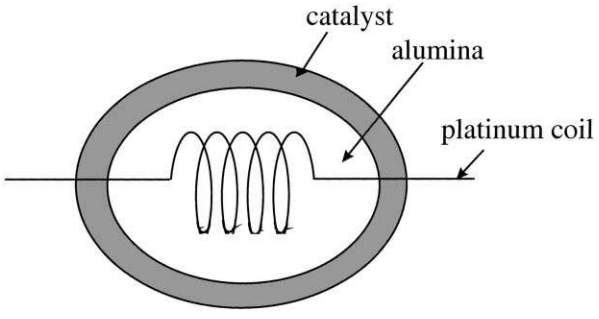

Fig. 26. Pellistor structure.

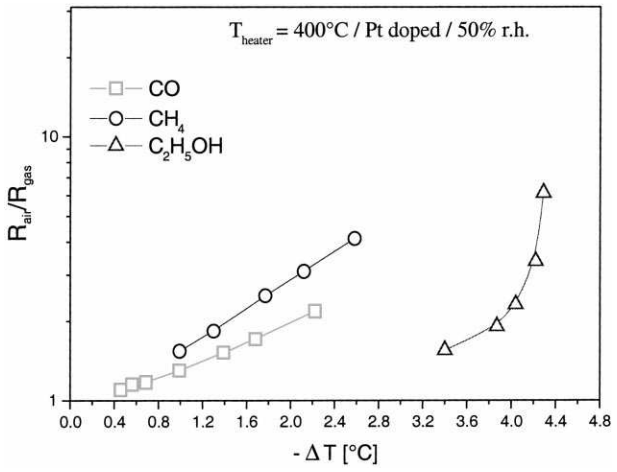

Fig. 27. Result from [82] showing the correlation between sensor signal, defined as R_{air}/R_{gas}, and temperature change dT for a Pt-doped micromachined SnO_2-sensor under exposure of CO (5–200 ppm), CH_4 (100–2000 ppm), C_2H_5OH (200–4000 ppm).

approach – electrodes, heater and temperature sensors function are all included in one Pt-coil – yields a sensor output signal which is a mixture of catalytic and heating effects as well as resistance changes of the metal oxide. The semistor offers, therefore, less information than a standard resistive sensor and one expects, therefore, a deteriorated instead of improved sensor performance of the semistor compared to a standard resistive sensor.

A better possibility to make use of catalytic effects might be the simultaneous measurement of resistance and temperature changes of a ``normal'' gas sensor where electrodes and heater are different structures. With the temperature measurement one can obtain additional information about the reactions at the sensor surface such that with both, resistance and temperature measurement, an improved sensor selectivity [82] can be obtained. An example is given in Fig. 27.

Rather unexpected is the observed temperature drop under exposure of reducing gases which has also been observed by Takada [83] for ceramic sensors and by Shin et al. [84] for a micromachined sensor. Due to the exothermic reaction of reducing gases with surface oxygen a temperature increase would have been expected. Up to now this phenomenon cannot be fully explained.

Takada [83] and Shin et al. [84] suggest that the temperature drop is caused by an increase in thermal conductivity of the sensing layer leading to an increase of heat losses to the substrate. They suppose that, if one considers the heat effects of all processes at the surface and not only the exothermic catalytic step, the temperature drop might be explained.

Even though the observed temperature changes are not fully understood the simultaneous measurement of temperature and resistive changes seem to offer a new way for sensor improvement. But, similar to the measurement of thermovoltages, one has to spent more effort in temperature control electronics than under solely resistance measurements. One has to find a way to differ between temperature changes caused by gas-specific reaction at the surface and those generated by a change of ambient temperature. A practical solution can be found following standard signal evaluation techniques of pellistors. Pellistors are in general operated together with a gas-insensitive reference element which possess the same thermal properties as the active sensor element and allows the compensation of ambient temperature changes simply by a Wheastone bridge [85,86].

Micromachined gas sensors are very promising for monitoring temperature changes: due to the good thermal isolation of the active area compared to ceramic sensors high temperature resolution can be achieved. The fast thermal response of micromachined gas sensors enables thereby fast monitoring of temperature changes. Reference elements for temperature compensation can simply be integrated on a micromachined substrate leading to well-matched sensor and reference elements. Therefore, micromachined gas sensors are for the measurement of temperature changes of advantage compared to ceramic-type sensors.

5. Conclusions

A variety of possibilities to fabricate micromachined substrates compatible with thin as well thick film metal oxide layers were presented. The advantages compared with the well-established ceramic sensors are: reduction of power consumption, faster thermal time constants which allow faster temperature modulations, the possibility to integrate the sensitive layer with control and signal evaluation electronic on one chip and easy integration of sensor arrays.

Thin and thick film sensing layers differ not only in their thickness but also in their microstructures and can thus lead to rather different transducer functions. This should be considered when searching for appropriate sensor output signals and operation modes, e.g. the presented electrode configurations and the application of electric fields seem only applicable to thin film layers. The simultaneous measurement of different sensor output signals such as sensor resistance, thermovoltage and heat of reaction can be used to obtain additional information about the surrounding gases. The same holds for sensor operation with modulated temperature. Plenty of possibilities are, therefore, given to search and find the right sensor output signal(s) and operation mode(s).

Further development of micromachined metal oxide sensors have to show whether these devices are stable also under field conditions and over the whole desired life-time. Stability has to be checked with respect to mechanical stability and sensor stability. A decision whether suspended type or closed membrane type devices are more appropriate cannot yet be made. The same holds also for thick versus thin film sensors. Up to now one can collect data about the sensitivity of thick and thin film sensors, but one can find only limited information about long term stability.

A lot more research will be necessary to obtain micromachined sensors which can be used in real applications but the starting points for such developments are drawn and the advantages of micromachined sensors are not only given with respect to sensor performance but also with respect to price. Micromachined metal oxide gas sensors might therefore play an important role to fulfill the demands of the market for low power, cheap and high performance devices.

References

[1] J.B.W.H. Brattain, Surface properties of germanium, Bell. Syst. Tech. J. 32 (1952) 1.

[2] T. Seiyama, A. Kato, K. Fujushi, M. Nagatani, A new detector for gaseous components using semiconductive thin films, Anal. Chem. 34 (1962) 1502f.

[3] N. Taguchi, Japenese Patent 45-38200.

[4] N. Taguchi, Japenese Patent 47-38840.

[5] N. Taguchi, US Patent 3 644 795.

[6] Figaro Products Catalogue, Figaro gas sensors 2000-series, Figaro Engineering Inc., European Office, Oststrasse 10, 40211 Djisseldorf, Germany.

[7] FIS, Product list (specifications: Sb/sp series), FIS incorporated, May 1999.

[8] UST, Product information, Umweltsensortechnik GmbH, Gewerbegebiet Geschwenda Süd Nr.3, D-98716 Geschwenda, 1999.

[9] K. Schierbaum, U. Weimar, W. Göpel, Multicomponent analysis: an analytical chemistry approach applied to modified SnO_2 sensors, Sens. Actuators B 2 (1990) 71–78.

[10] S. Fung, Z. Tang, P. Chan, J. Sin, P. Cheung, Thermal analysis and design of a micro-hotplate for integrated gas-sensor applications, Sens. Actuators A 54 (1996) 482–487.

[11] A. Götz, I. Gràcia, C. Canè, E. Lora-Taniayo, M. Horrillo, G. Getino, C. Gràcia, J. Gutiérrez, A micromachined solid state integrated gas sensor for the detection of aromatic hydrocarbons, Sens. Actuators B 44 (1997) 483–487.

[12] G. Sberveglieri, W. Hellmich, G. Müller, Silicon hotplates for metal oxide gas sensor elements, Microsyst. Technol. 3 (1997) 183–190.

[13] M. Hausner, J. Zacheja, J. Binder, Multi-electrode substrate for selectivity enhancement in air monitoring, Sens. Actuators B 43 (1997) 11–17.

[14] R. Cavicchi, J. Suehle, P. Chaparala, K. Kreider, M. Gaitan, S. Semancik, Micro-hotplate gas sensor, in: Proceedings of the 1994 Solid State Sensor and Actuator Workshop, Hilton Head, SC, USA, 1994, pp. 53–56.

[15] J. Gardner, A. Pike, N. de Rooji, M. Koudelka-Hep, P. Clerc, A. Hierlemann, W. Göpel, Integrated array sensor for detecting organic solvents, Sens. Actuators B 26/27 (1995) 135–139.

[16] D. Lee, W. Chung, M. Choi, J. Back, Low-power micro gas sensor, Sens. Actuators B 33 (1996) 147–150.

[17] P. Maccagnani, L. Don, P. Negrini, Thermo-insulated microstructures based on thick porous silicon membranes, in: Proceedings of the 13th European Conference on Solid-State Transducers, The Hague, The Netherlands, 12–15 September 1999, pp. 817–820.

[18] L. Sheng, Z. Tang, J. Wu, P. Clian, J. Sin, A low-power CMOS compatible integrated gas sensor using maskless tin oxide sputtering, Sens. Actuators B 49 (1998) 81–87.

[19] R. Cavicchi, J. Suehle, P. Chaparala, G. Poirier, K. Kreider, M. Gaitan, S. Semancik, Micro-hotplate temperature control for sensor fabrication, study, and operation, in: Proceedings of the Fifth International Meeting on Chemical Sensors, 1994, pp. 1136–1139.

[20] C. Dücsö, E. Vázsonyi, M. Ádám, I. Szabó, I. Bársony, J. Gardeniers, A. van den Berg, Porons silicon hulk micromachining for thermally isolated membrane formation, Sens. Actuators A 60 (1997) 235–239.

[21] J. Lim, H. Kim, B. Kang, D. Lee, Fabrication and characteristics of suspended-type micro gas sensor, J. Korean Phys. Soc. 33 (1998) 5432–5435.

[22] W. Chung, C. Shim, S. Choi, D. Lee, Tin oxide microsensor for LPG monitoring, Sens. Actuators B 20 (1994) 139–143.

[23] S. Semancik, R. Cavicchi, Kinetically controlled chemical sensing using micromachined structures, Accounts Chem. Res. 31 (5) (1997) 279–287.

[24] I. Stoev, D. Kohl, An integrated gas sensor on silicon substrate with sensitive SnO_x layer, Sens. Actuators B 2 (1990) 233–236.

[25] A. Götz, I. Gràcia, C. Canè, E. Lora-Tamayo, Thermal and mechanical aspects for designing micromachined low-power gas sensors, J. Micromech. Microeng. 7 (1997) 247–249.

[26] H. Tuller, R. Mlcak, Photo-assisted silicon micromachining: opportunities for chemical sensing, Sens. Actuators B 35/36 (1996) 255–261.

[27] P. Hille, H. Strack, A heated membrane for a capacitive gas sensor, Sens. Actuators A 32 (1992) 321–325.

[28] C. Saul, J. Zemel, Diode-based microfabricated hot-plate sensor, Sens. Actuators A 65 (1998) 128–135.

[29] S. Müller, J. Lin, E. Obermeier, Material and design considerations for lowpower microheater modules for gas-sensor applications, Sens. Actuators B 24/25 (1995) 343–346.

[30] D. Briand, B. van der Schoot, N. de Rooij, A. Krauss, U. Weimar, N. Bârsan, W. Göpel, High temperature micro-hotplates for drop coated gas sensors, in: Proceedings of the 13th European Conference on Solid-State Transducers, The Hague, The Netherlands, 12–15 September 1999, pp. 703–404.

[31] H. Baehr, K. Stephan, Wärme-und Stoffübertragung, 3rd Edition, Springer, Berlin, 1998.

[32] S. Astiè, A. Guè, E. Scheid, L. Lescouzéres, A. Cassagnes, Optimization of an integrated $Sn0_2$ gas sensor using a FEM simulator, Sens. Actuators A 69 (1998) 205–211.

[33] A. van Herwaarden, G. Meijer, Thermal sensors, in: S.M. Sze (Ed.), Semiconductor Sensors, Wiley, new York, 1994, Chapter 7, pp. 331–382.

[34] A. Götz, C. Canè, E. Lora-Tamayo, Specific problems of FEM thermal simulations for microsystems, in: Proceedings of the First International Conference on Simulation and Design of Microsystems and Microstructures microSiM, Vol. 95, 1995, pp. 137–1446.

[35] U. Grigull, H. Sandner, Wärmeleitung, Springer, Berlin, 1979.

[36] VDI-Wärmeatlas, VDI-Verlag Düsseldorf, 1994.

[37] H. Schlichting, K. Gersten, Grenzschicht-Theorie, Springer, Berlin, 1997.

[38] R. Aigner, M. Dietl, R. Katterloher, V. Klee, Si-planar-pellistor: design for temperature modulated operation, Sens. Actuators B 33 (1996) 151–155.

[39] V. Guidi, G Cardinali, L. Don, G. Faglia, M. Ferroni, G. Martinelli, P. Nelli, G. Sberveglieri, Thin-film gas sensor implemented on a low-power consumption micromachined silicon structure, Sens. Actuators B 49 (1998) 88–92.

[40] G. Meijer, A. Herwaarden, Thermal sensors, Sensors Series, Institute of Physics Publishing, Bristol and Philadelphia, 1994.

[41] C. Mastrangelo, W. Tang, Semiconductor sensor technologies, in: S. Sze (Ed.), Semiconductor Sensors, Wiley, 1994, Chapter 2, pp. 17–95.

[42] H. Low, M. Tse, M. Chiu, Thermal induced stress on the membrane in integrated gas sensor with micro-heater, in: Proceedings of the 1998 IEEE Hong Kong Electron Devices Meeting, 1990, pp. 140–143.

[43] C. Rossi, P. Temple-Boyer, D. Estéve, Realization and performance of thin SiO_2/SiN_x membrane for microheater applications, Sens. Actuators A 64 (1998) 241–245.

[44] J. Bosc, Y. Guo, V. Sarihan, T. Lee, Accelerated life testing for micro-machined chemical sensors, IEEE Trans. Reliability 47 (2) (1998) 135–141.

[45] W. Göpel, K. Schierbaum, SnO_2 sensors: current status and future prospects, Sens. Actuators B 26/27 (1995) 1–12.

[46] N. Yamazoc, New approaches for improving semiconductor sensors, Sens. Actuators B 5 (1991) 7–19.

[47] Y. Shimizu, M. Egashira, Basic aspects and challenges of semiconductor gas sensors, MRS Bulletin, 1999, pp. 16–24.
[48] J. McAleer, P. Mosley, J. Norris, D. Williams, Tin dioxide gas sensors, J. Chem. Soc., Faraday Trans. 1 83 (1987) 1323–1346.
[49] D. Williams, Semiconducting oxides as gas-sensitive resistors, Sens. Actuators B 57 (1999) 1–16.
[50] J. Watson, K. Ihokura, G. Coles, The tin dioxide gas sensor, Meas. Sci. Technol. 4 (1993) 711–719.
[51] W. Göpel, G. Reinhardt, Metal oxide sensors: new devices through tailoring interfaces on the atomic scale, in: H. Baltes, W. Göpel, J. Hesse (Eds.), Sensors Update, Vol. 1, VCH Weinheim, 1996, Chapter 2, pp. 47–120.
[52] G. Sberveglieri, Recent developments in semiconducting thin-film gas sensors, Sens. Actuators B 23 (1995) 103–109.
[53] N. Bârsan, M. Schweizer-Berberich, W. Göpel, Fundamental and practical aspects in the design of nanoscaled SnO_2 gas sensors: a status report, Fresenius J. Anal. Chem. 365 (4) (1999) 287–304.
[54] U. Weimar, W. Göpel, A.c. measurements on tin oxide sensors to improve selectivities and sensitivities, Sens. Actuators B 26/27 (1995) 13–18.
[55] V. Mishra, R. Agarwal, Effect of electrode material on sensor response, Sens. Actuators B 22 (1994) 121–125.
[56] R. Ionescu, A. Vancu, F. Buta, Diode-like SnO_2 gas detection devices, Sens. Actuators B 43 (1997) 126–131.
[57] M. Bauer, N. Bârsan, K. Ingrisch, A. Zeppenfeld, I. Denk, B. Schumann, U. Weimar, W. Göpel, Influence of measuring voltage and geometry of the sensing layer on the characteristics of thick film SnO_2 gas sensors, in: Proceedings of the 11th European Microelectronics Conference, 1997, pp. 37–44.
[58] U. Hoefer, H. Böttner, E. Wagner, C. Kohl, Highly sensitive NO_2 sensor device featuring a JFET-like transducer mechanism, Sens. Actuators B 47 (1998) 213–217.
[59] U. Hoefer, H. Böttner, A. Felske, G. Kühner, K. Steiner, G. Sulz, Thin-film SnO_2 sensor arrays controlled by variation of contact potential a suitable tool for chemometric gas mixture analysis in the TLV range, Sens. Actuators B 44 (1997) 429–433.
[60] U. Hoefer, K. Steiner, E. Wagner, Contact and sheet resistances of SnO_2 thin films from transmission-line-measurements, Sens. Actuators B 26/27 (1995) 59–63.
[61] W. Hellmich, G. Müller, C. Bosch-v.Braunmühl, T. Doll, I. Eisele, Field-effect-induced gas sensitivity changes in metal oxides, Sens. Actuators B 43 (1997) 132–139.
[62] M. Hausner, C. Hillebrecht, H. Karagözoglu, J. Zacheja, J. Binder, On-chip redundant measurement principles realized by a silicon sensor substrate, J. Micromech. Microeng. 7 (1997) 259–262.
[63] H.L. Vine, Method and apparatus for operating a gas sensor, US Patent 3906473 (September 1975).
[64] H. Eicker, Method and apparatus for determining the concentration of one gaseous component in a mixture of gases, US Patent 4012692 (March 1977).
[65] T. Oyabu, Y. Matuura, R. Murai, Carbon monoxide gas detector with shortened detecting cycle, Sens. Actuators B 1 (1990) 218–221.
[66] M. Jaegle, J. Wöllenstein, T. Meisninger, H. Böttner, G. Müller, T. Becker, C. Bosch-v.Braunmühl, Micromachined thin film SnO_2 gas sensors in temperature pulsed operation mode, Sens. Actuators B 57 (1999) 130–134.
[67] W. Sears, K. Colbow, F. Consadori, Algorithms to improve the selectivity of thermally-cycled tin oxide gas sensors, Sens. Actuators 19 (1989) 333–349.
[68] A. Lee, B. Reedy, Temperature modulation in semiconductor gas sensing, Sens. Actuators B 60 (1999) 35–42.
[69] T. Kunt, T. McAvoy, R. Cavicchi, S. Semancik, Dynamic modeling and optimization of micro-hotplate chemical gas sensors, in: Proceedings of the Advanced Control of Chemical Processes, 1997, pp. 91–95.
[70] T. Kunt, T. McAvoy, R. Cavicchi, S. Semancik, Optimization of temperature programmed sensing for gas identification using micro-hotplate sensors, Sens. Actuators B 53 (1998) 24–43.
[71] R. Cavicchi, J. Suehle, P. Chaparala, G. Poirier, K. Kreider, M. Gaitan, P. Chaparala, Optimized temperature-pulse sequences for the enhancement of chemically specific response patterns from micro-hotplate gas sensors, Sens. Actuators B 33 (1996) 142–146.
[72] A. Heilig, N. Bârsan, U. Weimar, M. Schweizer-Berberich, J. Gardner, W. Göpel, Gas identification by modulating temperatures of SnO_2-based thick film sensors, Sens. Actuators B 43 (1997) 45–51.
[73] S. Nakata, N. Ojima, Detection of a sample gas in the presence of an interferant gas based on a nonlinear dynamic response, Sens. Actuators B 56 (1999) 79–84.
[74] M. Schweizer-Berberich, S. Strathmann, U. Weimar, R. Sharma, A. Seube, A. Peyre-Lavigne, W. Göpel, Strategies to avoid VOC cross-sensitivity of SnO_2-based CO sensors, Sens. Actuators B 58 (1999) 318–324.
[75] K. Skrovan, Use of the Seebeck effect for sensing flammable gas and vapours, Sens. Actuators B 17 (1993) 13–17.
[76] R. Ionescu, Combined Seebeck and resistive SnO_2 gas sensors, a new selective device, Sens. Actuators B 48 (1998) 392–394.
[77] J. Miszei, H_2-induced surface and interface potentials on Pd-activated SnO_2 sensor films, Sens. Actuators B 28 (1995) 129–133.
[78] J. McAleer, P. Moseley, P. Bourke, J. Norris, R. Stephan, Tin dioxide gas sensors: use of the Seebeck effect, Sens. Actuators 8 (1985) 251–257.
[79] D. Vlachos, C. Papadopolous, J. Avaritsiotis, A technique for supressing ethanol interference employing Seebeck effect devices with carrier concentration modulation, Sens. Actuators B 44 (1997) 239–242.
[80] E. Jones, The pellistor catalytic gas sensor, in: P. Moseley, B. Tofield (Eds.), Solid state gas sensors, Hilger, Bristol, 1987, Chapter 2, pp. 17–31.
[81] G. Williams, G. Coles, The semistor: a new concept in selective methane detection, Sens. Actuators B 57 (1999) 108–114.
[82] A. Heilig, N. Bârsan, U. Weimar, W. Göpel, Selectivity enhancement of SnO_2 gas sensors: simultaneous monitoring of resistances and temperatures, in: Proceedings of the European Conference on Solid-State Transducers Eurosensors XII, 13–16 September 1998, pp. 633–636.
[83] T. Takada, Temperature drop of semiconductor gas sensor when exposed to reducing gases-Simultaneous measurement of changes in sensor temperature and in resistance, IMCS 98 (1998) 434–436.
[84] H. Shin, C. Lloyd, J. Gardner, Combined resistive and calorimetric sensing of gases using a single silicon micromachined device, Transducers 97 (1997) 935–938.
[85] P. Krebs, A. Grisel, A low power integrated catalytic gas sensor, Sens. Actuators B 13/14 (1993) 155–158.
[86] M. Zanini, J. Visser, L. Rimai, R. Soltis, A. Kovalchuk, D. Hoffman, E. Logothetis, U. Bonne, L. Brewer, O. Bynuin, M. Richard, Fabrication and properties of a Si-based high sensitivity microcalorimetric gas sensor, Soild State Sensor and Actuator Workshop, Hilton Head, SC, 1994, pp. 176–179.
[87] S. Sze, Semiconductor Sensors, Wiley, New York, 1994.
[88] H. Kuchling, Taschenbuch der Physik, 13th Edition, Verlag Harri Deutsch, 1991.
[89] Robert Bosch GmbH, Double-sensor element LGS2.
[90] G. Sberveglieri, Classical and novel techniques for the preparation of SnO_2 thin-film gas sensors, Sens. Actuators B 6 (1992) 239–247.
[91] M. Schweizer-Berberich, Gas sensors based on stannic oxide: material, design, performance, and modeling aspects, Dissertation, University of Tübingen, 1998.
[92] Gmelin, Zinn, Gmelin Handbuch der anorganischen Chemie, 8th Edition, Vol. Cl, 1972.
[93] Figaro Product Information, TGS 2201, Figaro Engineering Inc., European Office, Oststrasse 10, 40211 Dusseldorf, Germany.
[94] A. Heilig, Selektivitätssteigerung von S1102-Gassensoren, Dissertation, University of Tubingen, 1999.
[95] Figaro Products Catalogue, Figaro gas sensors 1-series 8-series, Figaro Engineering Inc., European Office, Oststrasse 10, 40211 Düsseldorf, Germany.
[96] Harald Boettner, personal communication.